1 **Title:** CCR4 and CCR7 differentially regulate thymocyte localization with distinct outcomes for central

2 tolerance

3 **Authors:** Yu Li[1†], Pablo Guaman Tipan[1†], Hilary J. Selden[1], Jayashree Srinivasan[1], Laura P. Hale[2], Lauren

4 I.R. Ehrlich[1,3 *]

5 [1] Department of Molecular Biosciences, The University of Texas at Austin, Austin, TX 78712, USA

6 [2] Department of Pathology, Duke University School of Medicine, Durham, NC 27710

7 [3] Department of Oncology, LIVESTRONG Cancer Institutes, The University of Texas at Austin Dell Medical

8 School, Austin, TX 78712, USA

9

10 [†] These authors contributed equally

11 [*] Correspondence: lehrlich@austin.utexas.edu (L.I.R. Ehrlich)

12

Abstract

Central tolerance ensures autoreactive T cells are eliminated or diverted to the regulatory T cell lineage, thus preventing autoimmunity. To undergo central tolerance, thymocytes must enter the medulla to test their TCRs for autoreactivity against the diverse self-antigens displayed by antigen presenting cells (APCs). While CCR7 is known to promote thymocyte medullary entry and negative selection, our previous studies implicate CCR4 in these processes, raising the question of whether CCR4 and CCR7 play distinct or redundant roles in central tolerance. Here, synchronized positive selection assays, 2-photon timelapse microscopy, and quantification of TCR-signaled apoptotic thymocytes, demonstrate that CCR4 and CCR7 promote medullary accumulation and central tolerance of distinct post-positive selection thymocyte subsets. CCR4 is upregulated within hours of positive selection signaling and promotes medullary entry and clonal deletion of immature post-positive selection thymocytes. In contrast, CCR7 is expressed several days later and is required for medullary localization and negative selection of mature thymocytes. In addition, CCR4 and CCR7 differentially enforce self-tolerance, with CCR4 enforcing tolerance to self-antigens presented by activated APCs, which express CCR4 ligands. Our findings show that CCR7 expression is not synonymous with medullary localization and support a revised model of central tolerance in which CCR4 and CCR7 promote early and late stages of negative selection, respectively, via interactions with distinct APC subsets.

Keywords: Thymocytes, Chemokine receptors, Negative selection, Central tolerance, *Ccr7*, *Ccr4*

Introduction

Self-tolerance of the T-cell repertoire is established in thymus through the process of central tolerance, which encompasses both negative selection and regulatory T cell (Treg) induction (Klein et al., 2014). To avoid autoimmunity, developing T cells must be broadly tolerized not only to ubiquitously expressed self-antigens, but also to proteins expressed by distinct differentiated cell types. The thymic medulla is a

36 specialized environment in which central tolerance to such diverse self-antigens is enforced. After
37 positive selection in the cortex, thymocytes migrate into the medulla, where they interact with
38 medullary antigen presenting cells (APCs), including thymic dendritic cells (DCs) and medullary thymic
39 epithelial cells (mTECs). Collectively, these APCs enforce self-tolerance by presenting self-peptides from
40 the majority of the proteome on MHC complexes, such that thymocytes expressing autoreactive T cell
41 receptors undergo clonal deletion or diversion to the Treg lineage (Ehrlich, 2016; Klein et al., 2014; Klein
42 et al., 2019; Lancaster et al., 2019). AIRE$^+$ mTECs express >80% of the proteome, including *Aire*-
43 dependent tissue restricted antigens (TRAs) that are otherwise expressed in only a few peripheral
44 tissues (Abramson & Anderson, 2017; Anderson & Su, 2016; Mathis & Benoist, 2007; Meredith et al.,
45 2015). DCs also present numerous self-antigens, including those acquired from mTECs, from circulation,
46 or from peripheral tissues and trafficked into the thymus (Atibalentja et al., 2009; Bonasio et al., 2006;
47 Koble & Kyewski, 2009). The importance of inducing thymocyte tolerance to medullary self-antigens is
48 evidenced by multi-organ autoimmunity that ensues in *Aire*-deficient mice and APECED patients
49 (Anderson et al., 2002; Finnish-German, 1997; Nagamine et al., 1997), in whom thymic expression of
50 TRAs is greatly diminished. Failure to express even a single medullary TRA can result in impaired
51 tolerance and subsequent T-cell mediated autoimmune pathology (DeVoss et al., 2006). Notably,
52 individual TRAs are expressed by only 1-3% of *Aire*$^+$ mTECs (Brennecke et al., 2015; Meredith et al.,
53 2015; Sansom et al., 2014), resulting in a sparse mosaic of self-antigen display throughout the medulla.
54 Because thymocytes reside in the medulla for only 4-5 days (McCaughtry et al., 2007), tight
55 spatiotemporal regulation is required to ensure that post-positive selection thymocytes encounter the
56 full spectrum of medullary self-antigens required to enforce self-tolerance.

57 To facilitate medullary entry after positive selection, thymocytes upregulate chemokine receptors that
58 promote their directional migration towards medullary-biased chemokine gradients (Bleul & Boehm,
59 2000; Hu, Lancaster, & Ehrlich, 2015; Lancaster et al., 2018; Petrie & Zuniga-Pflucker, 2007). Notably,

60 CCR7 has been shown to play a critical role in directing chemotaxis of post-positive selection thymocytes
61 towards the medulla, where CCR7 ligands are expressed, enhancing thymocyte accumulation within the
62 medulla, enforcing negative selection to TRAs, and averting autoimmunity (Ehrlich et al., 2009; Kozai et
63 al., 2017; Kurobe et al., 2006; Nitta et al., 2009; Ueno et al., 2004). Given the significance of CCR7 in
64 promoting thymocyte medullary entry, CCR7 expression is widely considered to be synonymous with
65 thymocyte medullary localization. Based largely on this definition, recent studies indicate that despite
66 the well-established role of the medulla in inducing central tolerance, ~75% of negative selection occurs
67 in $CCR7^-$ 'cortical' thymocytes, while only 25% occurs in $CCR7^+$ 'medullary' cells (Breed et al., 2019; Daley
68 et al., 2013; Hu et al., 2016). It has also been suggested that cortical negative selection may eliminate
69 thymocytes reactive to ubiquitous self-antigens while medullary deletion tolerizes TRA-responsive cells.
70 Our previous research implicates chemokine receptors other than CCR7 in promoting thymocyte
71 medullary localization (Ehrlich et al., 2009). We found that CCR4, which is upregulated by post-positive
72 selection thymocytes, also promotes medullary entry and negative selection (Hu, Lancaster,
73 Sasiponganan, et al., 2015). These findings raise the question of whether CCR4 and CCR7 play distinct or
74 redundant roles in promoting thymocyte medullary entry and central tolerance.

75 In this paper, we use a combination of approaches, including chemotaxis assays, 2-photon live-cell
76 microscopy, and synchronized positive selection assays, to distinguish the contributions of CCR4 versus
77 CCR7 to thymocyte medullary entry and negative selection. We find that CCR4 is upregulated by
78 thymocytes as early as a few hours after positive selection, while CCR7 is expressed days later by mature
79 post-positive selection cells. CCR4 expression promotes chemotaxis and medullary entry of early post-
80 positive selection thymocytes, which do not yet express CCR7. Initial CCR7 expression results in only
81 moderate thymocyte chemotaxis towards CCR7 ligands and modest accumulation in the medulla, such
82 that these thymocytes migrate in both the cortex and medulla. These findings indicate that CCR7
83 expression is not a definitive marker of medullary versus cortical localization. CCR7 is, however, required

84 for robust accumulation of mature (CD4SP) thymocytes in the medulla. Notably, consistent with their
85 differential activity in distinct thymocyte subsets, CCR4 and CCR7 are required in early and late phases of
86 polyclonal negative selection, respectively. While CCR7 is known to promote tolerance to TRAs (Kozai et
87 al., 2017; Nitta et al., 2009), we present evidence that CCR4 promotes tolerance to self-antigens
88 presented by activated APCs. Collectively, our study establishes non-redundant roles for CCR4 and CCR7
89 in governing localization of post-positive selection thymocyte subsets and central tolerance.

90 **Results**

91 **CCR4 is expressed by immature post-positive selection thymocyte subsets, while CCR7 expression is**
92 **restricted to more mature thymocyte subsets**

93 We first investigated expression of CCR4 and CCR7 by distinct thymocyte subsets using cell surface
94 markers that delineate developmental stages after positive selection (Figure 1A) (Sinclair et al., 2013;
95 Xing et al., 2016). To validate the developmental trajectory of these thymocyte subsets, we analyzed
96 their GFP expression levels in Rag2p-GFP mice, in which GFP expression is driven by the *Rag2* promoter.
97 In this model, expression of GFP distinguishes newly generated thymocytes (GFP^+) from recirculating T
98 cells (GFP^-), and declining GFP expression reflects time elapsed after positive selection, when the *Rag2*
99 promoter becomes inactive (Boursalian et al., 2004). In pre-positive selection $CD4^+CD8^+$ double-positive
100 (DP) $CD3^-CD69^-$ thymocytes, the *Rag2* promoter is active, resulting in maximal GFP expression (Figure
101 1B). After receiving a TCR signal, thymocytes upregulate CD3 and CD69 (Fu et al., 2009), generating early
102 post-positive selection DP $CD3^{lo}CD69^+$ cells; the brief time elapsed after positive selection is indicated by
103 continued high GFP expression by this subset (Figure 1B). To further evaluate if DP $CD3^{lo}CD69^+$
104 thymocytes represent post-positive selection thymocytes, as opposed to cells undergoing strong TCR
105 signaling driving clonal deletion, we evaluated thymocyte subsets from *Nur77*^{GFP} mice, in which GFP
106 levels reflect the strength of TCR signaling (Figure 1—figure supplement 1) (Moran et al., 2011).

107 Elevation of GFP expression by DP CD3^{lo}CD69^{+} cells, relative to DP CD3^{-}CD69^{-} cells, confirmed this subset
108 was TCR-signaled. Thymocytes rescued from negative selection express *Nur77^{GFP}* at levels comparable to
109 thymic Tregs, which express self-reactive TCRs (Stritesky et al., 2013). GFP levels were substantially
110 lower in DP CD3^{lo}CD69^{+} cells than in CD25^{+} CD4SPs, which are mostly Tregs (Figure 1—figure supplement
111 1A). Together, these data are consistent with DP CD3^{lo}CD69^{+} cells representing mainly post-positive
112 selection DPs, and not strongly self-reactive thymocytes undergoing negative selection. Sequential
113 maturation through by CD4^{+} single-positive semi-mature cells (CD4SP SM) and then CD4SP or CD8SP
114 mature 1 (M1) and mature 2 (M2) subsets was confirmed by progressive reductions in GFP levels for
115 both the CD4 and CD8 lineages (Figure 1B) (Xing et al., 2016). A distinct population of DP CD3^{+}CD69^{+}
116 cells expressed lower levels of GFP than CD4SP SM cells (Figure 1B), placing it temporally between
117 CD4SP SM and CD8SP M1 cells (Figure 1B). Thus, we considered whether DP CD3^{+}CD69^{+} cells represent
118 MHCI-restricted thymocytes in the process of differentiating into CD8SP cells through co-receptor
119 reversal downstream of the CD4SP SM stage (Brugnera et al., 2000). Consistent with this possibility, DP
120 CD3^{+}CD69^{+} cells were significantly reduced in *β2m$^{-/-}$* mice, in which positive selection of CD8SP
121 thymocytes is abrogated, as is selection of innate iNKT cells and CD8αα+ IELps (Bendelac et al., 1994;
122 Ruscher et al., 2017). Furthermore, DP CD3^{+}CD69^{+} cells were enriched in *MHCII$^{-/-}$* mice in which only
123 MHCI-restricted thymocytes are positively selected (Figure 1—figure supplement 1B-C)). Together, these
124 data demonstrate that DP CD3^{+}CD69^{+} cells are MHC-I restricted and have persisted for an intermediate
125 time between CD4SP SM and CD8SP M1 cells after positive selection, consistent with a co-receptor
126 reversing DP subset.

127 Having delineated the temporal sequence of thymocyte development post-positive selection, we
128 quantified expression of CCR4 and CCR7 by each subset. CCR4 is upregulated by the majority of early
129 post-positive selection DP CD3^{lo}CD69^{+} thymocytes, which do not yet express CCR7 (Figure 1C-D, Figure
130 1—figure supplement 2A-B). CCR7 is subsequently expressed at high levels by ~40% CD4SP SM cells, and

131 CCR4 expression persists on this subset (Figure 1C-D). In comparison to *Ccr7*$^{-/-}$ cells, low-level expression
132 of CCR7 can be detected on additional *Ccr7*$^{+/+}$ CD4SP SM cells, consistent with initial upregulation of
133 CCR7 by this subset (Figure 1—figure supplement 2A-B). Expression of CCR4 and CCR7 by MHCI-
134 restricted DP CD3^{+}CD69^{+} cells is similar to that of CD4SP SM cells, with slightly more CCR7 and less CCR4
135 (Figure 1C-D, Figure 1—figure supplement 2A-B). As thymocytes mature through CD4SP and CD8SP M1
136 and M2 stages, CCR4 is progressively downregulated. CCR7 expression peaks in both CD4SP and CD8SP
137 M1 subsets and is diminished in M2 cells (Figure 1C-D, Figure 1—figure supplement 2A-B). Because cell-
138 surface expression of CCR7 on mature CD4^{+} T cells can be downregulated due to ligand-induced
139 internalization of the chemokine receptor (Britschgi et al., 2008), we tested whether receptor
140 internalization could have obscured detection of CCR7 or CCR4 on ex vivo thymocyte subsets.
141 Thymocytes were incubated at 37°C for up to 2 hours, to allow re-expression of internalized receptors,
142 before immunostaining with anti-CCR7 and anti-CCR4 antibodies. Increased expression of cell-surface
143 CCR7 or CCR4 was not detected with increasing incubation time (Figure 1—figure supplement 2C-D).
144 These findings confirm that CCR4 expression is an early indicator of positive selection at the DP stage,
145 while CCR7 expression is upregulated later by more mature CD4SP and CD8SP subsets.

146 **Early post-positive selection thymocytes undergo chemotaxis towards CCR4 ligands, while more**
147 **mature subsets respond to CCR7 ligands**

148 We next determined whether expression of CCR4 and CCR7 corresponds to thymocyte chemotactic
149 responses to their respective ligands. DP CD3^{lo}CD69^{+} cells, which express CCR4 but not CCR7, underwent
150 chemotaxis in response to the CCR4 ligand CCL22, but not the CCR7 ligands CCL19 or CCL21 (Figure 2A-
151 D, Figure 2—figure supplement 1A). CCL22 induced chemotaxis of all subsequent post-positive selection
152 thymocytes, except the most mature M2 thymocyte subsets (Figure 2B, Figure 2—figure supplement
153 1A), largely in keeping with CCR4 expression patterns. Although CD4SP SM and DP CD3+CD69+ subsets
154 expressed CCR7 (Figure 1C), CCR7-mediated chemotaxis of these subsets did not reach statistical

155 significance when compared to all thymocyte subsets (Figure 2C-D). However, when considered
156 separately, moderate CCR7-mediated chemotaxis of these subsets was revealed, although DP
157 $CD3^{lo}CD69^{+}$ cells still did not undergo CCR7-mediated chemotaxis (Figure 2—figure supplement 1A).
158 Consistent with expression of CCR7 by more mature thymocyte subsets, the CCR7 ligands CCL19 and
159 CCL21 induced highly efficient chemotaxis of mature CD4SP and CD8SP M1 and M2 subsets (Figure 2C-
160 D).

161 A recent study indicated that expression of the chemokine receptor CXCR4 must be extinguished before
162 post-positive selection thymocytes can leave the cortex, where CXCL12 is expressed by cortical thymic
163 epithelial cells, to migrate into the medulla (Kadakia et al., 2019). Thus, we sought to place CXCR4
164 expression and function into context with CCR4 and CCR7. CXCR4 expression decreased after positive
165 selection, but all post-positive selection subsets continued to express CXCR4 (Figure 3A-B), and all
166 except for CD4SP SM and DP $CD3^{+}CD69^{+}$ subsets underwent chemotaxis in response to CXCL12 (Figure
167 3C). Although the earliest post-positive selection thymocyte subsets exhibited reduced CXCR4
168 responsiveness, perhaps allowing them to exit the cortex, the ability to respond to CXCR4 signals does
169 not preclude medullary localization, as evidenced by CXCR4-mediated chemotaxis of medullary CD4SP
170 and CD8SP M2 cells. Taken together, chemotaxis assays show that early post-positive selection DP
171 $CD3^{lo}CD69^{+}$ thymocytes are responsive to CCR4 but not CCR7 ligands, with low responsiveness to CXCR4
172 ligands. At the next stage, CD4SP SM cells also undergo chemotaxis towards CCR4 ligands, and begin to
173 migrate at a low level towards CCR7 ligands, but not to CXCR4 ligands. As thymocytes mature to the
174 CD4SP and CD8SP M1 and M2 stages, they progressively gain the ability to respond robustly to CCR7
175 ligands, regain CXCR4 responsiveness, and lose responsiveness to CCR4 ligands (Figure 3D).

176 Initial expression of CCR7 by CD4SP SM thymocytes does not result in strong chemotaxis to CCR7 ligands
177 (Figure 2D), and expression of CXCR4 by this subset does not enable detectable chemotaxis towards
178 CXCL12 (Figure 3C), highlighting a temporal disconnect between chemokine receptor expression and

179 function on maturing post-positive selection thymocytes. We considered the possibility that CD4SP SM
180 cells could be intrinsically unable to respond to chemokine receptor signaling. However, these cells
181 responded efficiently to CCR4 ligands (Figure 2B), and they underwent chemotaxis to the CCR9 ligand
182 CCL25 at levels comparable to DP $CD3^{lo}CD69^{+}$ cells (Figure 2—figure supplement 2A), consistent with a
183 previous study showing CCL25 induces migration of most thymocyte subsets (Campbell et al., 1999).
184 Thus, regulation of thymocyte responsiveness to chemokine receptors is more complex than altered
185 cell-surface expression levels.

186 CCL21a establishes a chemokine gradient that drives accumulation of CD4SP thymocytes in the medulla
187 (Kozai et al., 2017; Ueno et al., 2002; Ueno et al., 2004). Because we found that functional CCR4 is
188 expressed by early post-positive selection DP thymocytes, we examined whether CCL22 could establish a
189 similar chemokine gradient to recruit these CCR4-responsive cells into the medulla.
190 Immunofluorescence analysis revealed that CCL22 is expressed predominantly in the medulla (Figure
191 2—figure supplement 2B), consistent with a potential role in inducing medullary entry of early post-
192 positive selection thymocytes.

193 **The timing of CCR4 upregulation following positive selection correlates with thymocyte medullary**
194 **entry**

195 Given that the majority of early post-positive selection DP thymocytes respond to CCR4 but not CCR7
196 ligands, we sought to determine how rapidly CCR4 versus CCR7 are upregulated following initiation of
197 positive selection and to assess whether expression of either receptor correlates with the timing of
198 medullary entry. To accomplish these goals, we used a synchronized positive selection thymic slice
199 assay, coupled with flow cytometry or 2-photon microscopy (Figure 4A). OT-II^{+} *Rag2*$^{-/-}$ *MHCII*$^{-/-}$ mice
200 served as a source of pre-positive selection DP thymocytes that did not yet express CCR4 or CCR7 due to
201 lack of positive selection in the absence of MHCII expression (Figure 4B). OT-II^{+} *Rag2*$^{-/-}$ *MHCII*$^{-/-}$

202 thymocytes were fluorescently labeled prior to culturing on MHC-II-sufficient, positively selecting (wild-
203 type (WT or pCX-EGFP) or non-positively selecting (*MHCII*$^{-/-}$) live thymic slices. At various time points,
204 expression of CCR4 and CCR7 by OT-II thymocytes in the thymic slices was assayed by flow cytometry, or
205 medullary entry was quantified by 2-photon live-cell microscopy (Figure 4A).

206 OT-II^{+} *Rag2*$^{-/-}$ *MHCII*$^{-/-}$ DP cells upregulated CCR4 as early as 3 hours (3h) after being introduced onto
207 positively selecting thymic slices (Figure 4C). The frequency of CCR4^{+} cells continued to increase over 24
208 hours on WT slices. Positive selection was required for initiation of CCR4 expression, as demonstrated by
209 the failure to upregulate CCR4 on non-selecting *MHCII*$^{-/-}$ slices. CCR7 was not upregulated within 24h of
210 initiating positive selection (Figure 4C). When labeled OT-II^{+} *Rag2*$^{-/-}$ *MHCII*$^{-/-}$ thymocytes were introduced
211 into positively selecting pCX-EGFP thymic slices and imaged by 2-photon microscopy, they were initially
212 localized to the cortex, consistent with our previous findings that pre-positive selection thymocytes
213 cannot access the medulla (Video S1) (Ehrlich et al., 2009). By 9-12 hours after positive selection, OT-II^{+}
214 thymocytes entered the medulla, as evidenced by a significant increase in medullary density (Figure 4D-
215 E; Video S2). As CCR7 is not yet expressed by these cells (Figure 4C), CCR4 likely drives medullary entry
216 of early post-positive selection thymocytes.

217 To test if the timing of CCR4 and CCR7 upregulation and medullary entry are comparable for MHCI-
218 restricted thymocytes, we carried out similar experiments using pre-positive selection OT-I^{+} *Rag2*$^{-/-}$
219 thymocytes that matured in the non-selecting thymuses of *β2m*$^{-/-}$ hosts. Although OT-I positive selection
220 was largely inhibited in these bone marrow chimeras, about 10% of the DP cells expressed CCR4 at
221 baseline (Figure 4—figure supplement 1A-B). Nonetheless, CCR4 was upregulated as early as 3h after
222 initiating positive selection in WT thymic slices, but not in non-selecting *β2m*$^{-/-}$ slices and increased over
223 24 hours (Figure 4—figure supplement 1A-B). CCR7 was not expressed during the first 24h after
224 initiation of positive selection and only became detectable as CD8SP cells differentiated at the 72h

225 timepoint (Figure 4—figure supplement 1 B-C), consistent with prior observations (Lutes et al., 2021).
226 Furthermore, 2-photon imaging of pre-selection OT-I^{+} *Rag2*$^{-/-}$ thymocytes within the cortex and medulla
227 of thymic slices showed that despite medullary entry of some thymocytes at 1.5h (Video S3), likely due
228 to the observed baseline CCR4 expression in this model, the medullary density of OT-I thymocytes
229 increased significantly by 12h after the initiation of positive selection (Figure 4—figure supplement 1 D-
230 E; Video S4).

231 Together, these findings show that both MHCI- and MHCII-restricted thymocytes upregulate CCR4
232 within a few hours of the initiation of positive selection and accumulate significantly in the medulla by 9-
233 12h. Thymocyte medullary entry precedes CCR7 upregulation, which does not occur until 48h-72h after
234 positive selection. The kinetics of CCR4 upregulation are consistent with a role for CCR4 in promoting
235 early medullary entry of positively selected thymocytes. However, CCR7 is known to be required for
236 efficient medullary entry of SP thymocytes (Ehrlich et al., 2009; Kurobe et al., 2006), raising the
237 possibility that these two chemokine receptors promote medullary localization of different thymocyte
238 subsets.

239 **CCR4 and CCR7 are required for medullary accumulation of distinct post-positive selection thymocyte**
240 **subsets**

241 To test our hypothesis that CCR4 and CCR7 are required for medullary accumulation of distinct post-
242 positive selection thymocytes, we FACS purified thymocyte subsets from WT, *Ccr4*$^{-/-}$, *Ccr7*$^{-/-}$ and *Ccr4*$^{-/-}$
243 *Ccr7*$^{-/-}$ (DKO) mice, labeled them with red or blue fluorescent dyes, and allowed them to migrate in pCX-
244 EGFP live thymic slices. 2-photon time-lapse microscopy was used to image the sorted cells, so we could
245 determine their migratory properties and densities in the medulla versus cortex (Figure 5—figure
246 supplement 1A). EGFP is expressed ubiquitously in pCX-EGFP mice, such that the cortex and medulla of

247 thymic slices can be distinguished by differences in stromal cell morphology and EGFP intensity (Figure
248 5A) (Ehrlich et al., 2009).

249 Purified WT DP CD3^{lo}CD69^{+} cells entered and migrated within the medulla, accumulating at a 2-fold
250 higher density than in the cortex (Figure 5A-B; Video S5). As expected, the majority of the sorted early
251 post-positive selection cells expressed CCR4, but not CCR7 (Figure 5—figure supplement 1B-C).
252 Medullary enrichment of this subset was abolished when the cells were purified from *Ccr4*$^{-/-}$ or DKO
253 mice, but *Ccr7* deficiency did not diminish their medullary accumulation (Figure 5B). Paired analyses of
254 WT versus *Ccr4*$^{-/-}$ and *Ccr7*$^{-/-}$ versus DKO DP CD3^{lo}CD69^{+} cells imaged together in the same slices
255 confirmed that *Ccr4* deficiency significantly impaired medullary accumulation of this early post-positive
256 selection DP subset irrespective of *Ccr7* genotype, but genetic deficiency of *Ccr7* at this stage did not
257 alter medullary accumulation (Figure 5C). Altogether, CCR4 is required for the 2-fold accumulation of DP
258 CD3^{lo}CD69^{+} cells in the medulla relative to the cortex.

259 Despite the fact that roughly half of the purified CD4SP SM cells expressed CCR7 (Figure 5—figure
260 supplement 1B-C), which is considered to be a hallmark of thymocyte medullary entry, accumulation of
261 these cells within the medulla did not further increase, but instead remained at a 2-fold medullary:
262 cortical density ratio, comparable to that of DPCD3^{lo}CD69^{+} cells (Figure 5A-B; Video S6). Medullary
263 accumulation of this subset was significantly reduced by CCR4 deficiency, regardless of the *Ccr7*
264 genotype (Figure 5B-C), indicating an important role for CCR4 in promoting medullary localization of
265 CD4SP SM cells. In addition, paired analysis of *Ccr7*$^{-/-}$ versus WT CD4SP SM cells imaged together in the
266 same slices showed that CCR7 also contributes to medullary accumulation of CD4SP SM cells (Figure 5C).
267 Together, these data indicate that CCR4 and CCR7 cooperate to promote medullary accumulation of
268 CD4SP SM thymocytes.

269 CD4SP M1+M2 thymocytes, the majority of which express only CCR7 (Figure 5—figure supplement 1C),
270 accumulated in the medulla to a greater extent than either of the previous subsets, with a ~4-5-fold
271 medullary:cortical density ratio (Figure 5B-C; Video S7, S8), consistent with the high migration index of
272 these cells to CCR7 ligands (Figure 2C-D). CCR4 deficiency did not significantly impact medullary
273 accumulation of this subset (Figure 5B-C), consistent with the lack of responsiveness of M2 cells to CCR4
274 ligands (Figure 2A). However, the trend towards decreased medullary enrichment of *Ccr4* deficient cells
275 may reflect the activity of CCR4 in CD4SP M1 cells (Figure 2A). Medullary accumulation of M1+M2
276 CD4SP thymocytes was highly dependent on CCR7, as demonstrated by the significant decrease in
277 medullary accumulation of both *Ccr7*$^{-/-}$ and DKO cells relative to WT or *Ccr4*$^{-/-}$ cells (Figure 5B, Video S7,
278 S8).

279 We also considered whether CCR4 and CCR7 alter thymocyte migratory properties. Deficiency in *Ccr4*
280 and/or *Ccr7* did not impact the speed of DP CD3^{lo}CD69^{+} or CD4SP SM cells. However, CCR7 deficiency
281 resulted in a significant decline in the speed of CD4SP M1+M2 cells, consistent with our previous finding
282 that CCR7 promotes rapid motility of CD4SP thymocytes (Ehrlich et al., 2009). Interestingly, double
283 deficiency of *Ccr4* and *Ccr7* resulted in a significant increase in the average path straightness of all
284 imaged thymocyte subsets (Figure 5E), suggesting that thymocytes responding to CCR4 and CCR7 ligands
285 migrate in a more tortuous path.

286 Overall, CCR4 and CCR7 were required for medullary accumulation of distinct post-positive selection
287 thymocyte subsets, largely consistent with their expression patterns and chemotactic function (Figure
288 3D). Notably, our results show that CCR4 directs early post-positive selection thymocytes into the
289 medulla, demonstrating that lack of CCR7 expression by post-positive selection thymocytes does not
290 preclude medullary localization. Conversely, expression of CCR7 by CD4SP SM cells does not result in
291 enhanced medullary accumulation over the previous subset. Thus, CCR7 expression on its own is not

292 indicative of robust medullary accumulation. Interestingly, only mature CD4SP M1+M2 cells accumulate
293 robustly in the medulla and migrate rapidly in a CCR7-dependent manner.

294 **CCR4 and CCR7 contribute to early versus late phases of negative selection, respectively**

295 Given the differential impact of CCR4 versus CCR7 on migration and medullary accumulation of post-
296 positive selection thymocyte subsets, we hypothesized that these chemokine receptors are required for
297 negative selection of early versus late post-positive selection cells, respectively. Consistent with our
298 prior observations (Hu, Lancaster, Sasiponganan, et al., 2015), the frequencies of post-positive selection
299 thymocyte subsets were comparable between littermate control WT and *Ccr4*$^{-/-}$ mice (Figure 6—figure
300 supplement 1A). CD5 expression levels, which are a proxy for self-reactivity (Azzam et al., 1998; Hawiger
301 et al., 2004; Persaud et al., 2014), were also comparable in the absence of *Ccr4* (Figure 6—figure
302 supplement 1). To test the impact of CCR4 and CCR7 on polyclonal negative selection, we quantified the
303 frequency of cleaved-caspase 3^{+} thymocytes that had undergone TCR signaling in WT, *Ccr4*$^{-/-,}$ *Ccr7*$^{-/-}$, and
304 DKO mice. Intracellular cleaved-caspase 3 in TCR-signaled thymocytes has been shown to mainly reflect
305 negative selection (Breed et al., 2019; Hu et al., 2016), although other apoptotic stimuli, such as
306 glucocorticoid hormones, could also induce cleaved-caspase 3 in thymocytes (Alam et al., 1997;
307 Marchetti et al., 2003). Previous studies showed that negative selection occurs in 2 main phases,
308 generally defined to occur at the CCR7^{-} DP stage in the cortex versus the CCR7^{+} CD4SP stage in the
309 medulla (Breed et al., 2019; Daley et al., 2013; Hu et al., 2016; Stritesky et al., 2013). Thus, we
310 quantified the impact of *Ccr4* versus *Ccr7* deficiency on “early-phase” and “late-phase” negative
311 selection (Figure 6A-B). Interestingly, the majority of early-phase DP cells undergoing negative selection
312 expressed only CCR4, as did ~60% of late-phase CD4SP cells; thus, the majority of thymocytes
313 undergoing clonal deletion express CCR4, but not CCR7. CCR7 was expressed by ~40% CD4SP and 60% of
314 CD8SP cells undergoing negative selection (Figure 6B). The frequency of total thymocytes undergoing
315 negative selection declined significantly only in DKO mice (Figure 6C). However, CCR4 deficiency resulted

316 in a significant decrease in the frequency of thymocytes undergoing early-phase, but not late-phase
317 negative selection (Figure 6C). In contrast, CCR7 deficiency resulted in a significantly lower frequency of
318 thymocytes undergoing late-phase negative selection, with no impact on early-phase negative selection.
319 Double-deficiency for CCR4 and CCR7 significantly diminished both early-phase and late-phase negative
320 selection (Figure 6C). It was reported that most negative selection occurs at the earlier phase (Breed et
321 al., 2019; Stritesky et al., 2013), which is consistent with the 2:1 ratio of WT thymocytes undergoing
322 early- to late-phase negative selection (Figure 6D). This ratio falls significantly in *Ccr4*$^{-/-}$ mice and
323 increases significantly in *Ccr7*$^{-/-}$ and DKO mice, highlighting the respective contributions of CCR4 and
324 CCR7 to early versus late phases of negative selection, respectively (Figure 6D). Altogether, these data
325 indicate that, consistent with its role in promoting medullary entry of early-post positive selection
326 thymocytes, CCR4 is required for efficient early-phase negative selection of polyclonal DP cells. In
327 contrast, CCR7, which promotes medullary accumulation of more mature CD4SP and CD8SP cells, is
328 required for efficient negative selection of late-phase CD4SP and CD8SP cells.

329 **CCR4 and CCR7 suppress autoinflammation in distinct tissues, with CCR4 promoting tolerance to**
330 **activated antigen-presenting cells**

331 Given that CCR4 and CCR7 enforced central tolerance at distinct stages of T-cell development when
332 thymocytes might interact with different APCs, these chemokine receptors could promote tolerance to
333 distinct self-antigens. To evaluate this possibility, we assessed the presence of spontaneous
334 autoimmunity/autoinflammation in multiple organs of WT, *Ccr4*$^{-/-}$, *Ccr7*$^{-/-}$ and *Ccr4*$^{-/-}$*Ccr7*$^{-/-}$mice. We
335 previously found that *Ccr4*$^{-/-}$ and *Ccr7*$^{-/-}$ mice had anti-nuclear autoantibodies by ~12-months of age (Hu
336 et al., 20115). Here we detected anti-nuclear autoantibodies in the serum of 67% of *Ccr4*$^{-/-}$,100% of
337 *Ccr7*$^{-/-}$*, and 75% of Ccr4*$^{-/-}$*Ccr7*$^{-/-}$ *mice* between 5 to 6.5 months of age, relative to 22% of WT mice (Figure
338 7—figure supplement 1A). Thus, we evaluated other organs from mice in this age range for lymphocytic
339 infiltrates or inflammation. Colon inflammation was not observed in *Ccr7*$^{-/-}$ or WT mice. Colons from

340 *Ccr4*$^{-/-}$ mice showed mild epithelial hyperplasia, with small foci of acute inflammation. In contrast, Ccr4$^{-/-}$
341 *Ccr7*$^{-/-}$ mice demonstrated moderate to severe colonic mucosal hyperplasia, with abundant acute and
342 chronic inflammation extending into the submucosa. Active ulcerations were observed in 40% of *Ccr4*$^{-/-}$
343 *Ccr7*$^{-/-}$ mice, with crypt abscesses and regenerative changes consistent with prior ulceration in most
344 *Ccr4*$^{-/-}$ *Ccr7*$^{-/-}$ mice (Figure 7A, left). Histologic scores were markedly and significantly higher in *Ccr4*$^{-/-}$
345 *Ccr7*$^{-/-}$ mice compared to WT, with a trend toward higher scores in *Ccr4*$^{-/-}$ mice that is absent in *Ccr7*$^{-/-}$
346 mice (Figure 7A, right), suggesting that CCR4 and CCR7 collaboratively maintain self-tolerance in the
347 colon (Figure 7A). Immune infiltrates were elevated in the liver, lacrimal glands, and submandibular
348 glands of *Ccr7*$^{-/-}$ and *Ccr4*$^{-/-}$*Ccr7*$^{-/-}$ mice, but not *Ccr4*$^{-/-}$ mice at 6-months of age (Figure 7B, Figure 7- figure
349 supplement 1B-D), indicating that CCR7 plays a dominant role in promoting tolerance to endocrine
350 organs, consistent with the established requirement for CCR7 to mediate negative selection against
351 mTEC-expressed TRAs, but not ubiquitous self-antigens (Nitta et al., 2009). Interestingly, 70-75% of *Ccr4*$^{-}$
352 $^{/-}$ mice, compared to 17-20% of WT and 0% of *Ccr7*$^{-/-}$ mice displayed moderate lymphoid hyperplasia in
353 the spleen and mesenteric lymph nodes of 12-month old mice (Figure 7C, right). Immunofluorescent
354 staining of lymph nodes from 6-month old *Ccr4*$^{-/-}$ mice revealed abnormal CD4 and CD8
355 distributions/expansions in T-cell zones relative to WT mice (Figure 7C, left). As expected, T cell zones
356 from *Ccr7*$^{-/-}$ mice were hypoplastic (not shown), reflecting the role of CCR7 in mediating T-cell entry into
357 LNs. These results indicate that CCR4 maintains T cell homeostasis in secondary lymphoid organs.

358 Given the distinct contributions of CCR4 and CCR7 to establishment of central tolerance and
359 maintenance of self-tolerance across different organs, we considered the possibility that CCR4 and CCR7
360 might promote thymocyte selection against antigens presented by different types of thymic APCs.
361 Thymic APC subsets were FACS purified (Figure 7—figure supplement 2A), and expression of CCR4 and
362 CCR7 ligands was quantified by qRT-PCR. Consistent with our previous study (Hu, Lancaster,
363 Sasiponganan, et al., 2015), the CCR4 ligands CCL17 and CCL22 were expressed by Sirpα^{+} cDC2 cells.

364 Activated thymic CCR7^{+} cDCs (Ardouin et al., 2016; Hu et al., 2017; Oh et al., 2018) also expressed CCR4
365 ligands, with the highest levels of CCL22 expressed by activated DCs (Figure 7D). Thymic B cells also
366 expressed CCL22, consistent with a recent report that CCL22 expressed by activated B cells promotes
367 interactions with T cells in the germinal center (Liu et al., 2021). The CCR7 ligands CCL19 and CCL21 were
368 expressed by mTEC subsets, with the highest levels of CCL21 expression by mTEC^{lo} cells (Figure 7E),
369 consistent with previous reports (Bornstein et al., 2018; Kozai et al., 2017). These results suggest that
370 CCR4 may promote thymocyte interactions with B cells and cDCs, including activated CCR7^{+} cDCs that
371 express elevated levels of MHCII and co-stimulatory molecules (Ardouin et al., 2016; Hu et al., 2017),
372 while CCR7 may promote thymocyte interactions primarily with mTECs.

373 Because a large proportion of thymic B cells (Cepeda et al., 2018) and cDCs (Ardouin et al., 2016; Hu et
374 al., 2017) have activated phenotypes, and T-cell zones in the lymph nodes of *Ccr4*$^{-/-}$ mice are
375 hyperplastic (Figure 7C), we considered the possibility that CCR4-directed negative selection could
376 facilitate establishment of central tolerance to antigens expressed by activated APCs. To explore this
377 hypothesis, CD45.1^{+} congenic splenocytes were stimulated overnight with toll-like receptor (TLR)
378 ligands. We confirmed that stimulation with TLR ligands induced activation of the splenic cDCs and B
379 cells based on upregulation of MHCII, CD80, and CD86 (Figure 7—figure supplement 2B). The activated
380 splenocytes were then co-cultured with CD45.2^{+} CD4^{+} conventional T cells isolated from WT or *Ccr4*$^{-/-}$
381 spleens, and the frequency of T cells induced to proliferate was quantified after 3-5 days (Figure 7F).
382 Notably, LPS-stimulated splenocytes induced more proliferation of *Ccr4*$^{-/-}$ versus WT CD4^{+} T cells at days
383 3 and 5 (Figure 7G). Splenocytes that were unstimulated or activated by other TLR ligands did not
384 preferentially induce *Ccr4*$^{-/-}$ T cell proliferation (Figure 7E, Figure 7—figure supplement 2C). Taken
385 together, these data suggest that CCR4 promotes thymocyte central tolerance to self-antigens
386 expressed by LPS-activated APCs, possibly by promoting interactions with such APCs in the thymus.

387 **Discussion**

388 Our data demonstrate that CCR4 and CCR7 play distinct roles in thymocyte localization and the
389 induction of T-cell central tolerance. We find that CCR4 is upregulated by thymocytes within a few hours
390 of the initiation of positive selection, largely coincident with the timing of medullary entry. CCR4 is
391 expressed by almost all early post-positive selection DP $CD3^{lo}CD69^{+}$ cells and is required for their 2-fold
392 accumulation in the medulla and efficient negative selection. Notably, the majority of thymocytes
393 undergoing negative selection are DP $CD3^{lo}CD69^{+}$ cells, which do not express CCR7. Thus, while the role
394 of CCR4 in negative selection has been questioned (Cowan et al., 2014), our analyses reveal an
395 important role for this chemokine receptor in localization and central tolerance of early post-positive
396 selection polyclonal thymocytes, in keeping with medullary localization of the CCR4 ligand CCL22. In
397 contrast, our study and a previous report (Lutes et al., 2021) show that CCR7 is not upregulated until 48-
398 72 hours after positive selection. CCR7 is expressed by about half of the CD4SP SM cells, which continue
399 to express CCR4 and respond to CCR4 ligands. In keeping with dual expression, CCR4 and CCR7
400 cooperate to induce the 2-fold accumulation of CD4SP SM cells in the medulla. As thymocytes mature
401 further to the CD4SP and CD8SP M1 and M2 stages, CCR7 is upregulated, CCR4 is downregulated, and
402 the cells become increasingly chemotactic to CCR7 ligands. We find that CCR7 is required for the robust
403 accumulation of CD4SP M1+M2 cells in the medulla and for late-phase negative selection of CD4SP and
404 CD8SP thymocytes. The finding that the overall frequency of negative selection in the thymus is reduced
405 significantly only in the absence of both CCR4 and CCR7 further indicates that these chemokine
406 receptors both contribute to the induction of central tolerance. Altogether, our findings show a
407 temporally correlated shift after positive selection from a requirement for CCR4 to a requirement for
408 CCR7 for thymocyte medullary localization and negative selection.

409 Several of our findings raise questions about the current model of negative selection, which assumes
410 that CCR7 expression is a surrogate indicator of thymocyte medullary versus cortical localization (Breed
411 et al., 2019; Hu et al., 2016). This assumption is based on studies, including our own, showing that CCR7

412 is expressed by CD4SP and CD8SP thymocytes, which are localized mainly within the thymic medulla at
413 steady-state, as evidenced by immunostaining (Ehrlich, 2016). In addition, prior studies showed that
414 accumulation of CD4SP cells in the medulla is CCR7-dependent (Ehrlich et al., 2009; Ueno et al., 2004);
415 consistent with these findings, we confirm that robust medullary accumulation of the more mature
416 CD4SP M1 and M2 cells is CCR7-dependent. Equating CCR7 expression with medullary localization has
417 led to a model in which the early phase of negative selection is thought to impact CCR7^{-} DP cells in the
418 cortex, while the later phase impacts more mature CCR7^{+} cells in the medulla (Breed et al., 2019; Hu et
419 al., 2016). In support of cortical negative selection, apoptotic TCR transgenic cells were located in the
420 cortex of the H-Y^{CD4} model of negative selection (McCaughtry et al., 2008). Also, TCR-signaled
421 thymocytes are present at the cortical side of the CMJ in *Bim*$^{-/-}$ mice, in which apoptosis following strong
422 TCR signaling is impaired (Stritesky et al., 2013), suggesting thymocytes encounter negatively selecting
423 self-antigens in the cortex. Furthermore, CCR7 deficiency impairs negative selection to TRAs, but not to
424 ubiquitous self-antigens (Kurobe et al., 2006; Nitta et al., 2009), indicating that CCR7^{+} mature
425 thymocytes undergo negative selection in the medulla, where TRAs are expressed by mTECs.

426 While our data confirm that CCR7 is critical for medullary accumulation of more mature thymocyte
427 subsets, we find that CCR7 expression is not a reliable indicator of medullary localization in earlier post-
428 positive selection thymocytes. CCR7^{-} DP CD3^{lo}CD69^{+} enter the medulla, where they accumulate in a
429 CCR4-dependent manner with a 2-fold higher density than in the cortex, so CCR7 is not required for
430 medullary entry. Conversely, although almost half of CD4SP SM cells express CCR7, their medullary:
431 cortical density is also 2-fold. CCR7 deficiency only modestly diminished medullary accumulation of
432 CD4SP SM cells, consistent with their moderate chemotaxis towards CCR7 ligands; instead, CCR4 played
433 a greater role in medullary accumulation of this subset. Thus, the two earliest post-positive selection
434 subsets accumulate in the medulla at similar densities, despite CCR7 upregulation by one of these
435 subsets. DP CD3^{lo}CD69^{+} and CD4SP SM cells both migrate in the cortex and in the medulla and could

436 thus encounter APCs presenting cognate self-antigens that drive negative selection in either region.
437 Based on the 2-fold enrichment of DP $CD3^{lo}CD69^{+}$ cells in the medulla, a substantial proportion of $CCR7^{-}$
438 early phase negative selection may occur in the medulla. Moreover, some late phase negative selection,
439 defined by either CCR7 expression or maturation to the CD4SP SM stage, may occur in the cortex. These
440 data indicate that CCR7 expression cannot be used as a reliable surrogate biomarker of medullary
441 localization. The location in which thymocytes undergo negative selection impacts which APC subsets
442 will be encountered, altering the spectrum of self-antigens to which thymocytes are tolerized. Thus, it
443 will be important to determine where distinct thymocyte subsets undergo negative selection and which
444 APCs promote tolerance of these different subsets.

445 It has recently been suggested that CXCR4 expression must be extinguished after positive selection to
446 release thymocytes from binding to cTECs in the cortex, thus enabling medullary entry (Kadakia et al.,
447 2019). However, we found that while CXCR4 is partially downregulated on the cell surface of post-
448 positive selection thymocytes, all subsets except CD4SP SM and DP $CD3^{+}CD69^{+}$ cells undergo chemotaxis
449 to CXCL12, despite their accumulation in the medulla. These findings indicate that CXCR4 expression and
450 activity are compatible with medullary localization. This seeming discrepancy may reflect the
451 overexpression system used to reveal that persistent CXCR4 expression prevented thymocyte medullary
452 entry, perhaps resulting in superphysiological tethering of cells to the cortex (Kadakia et al., 2019). In
453 keeping with the ability of $CXCR4^{+}$ thymocytes to enter the medulla, higher CXCR4 surface expression
454 and responsiveness are observed in mature CD4SP and CD8SP M1 and M2 subsets, which accumulate in
455 the medulla to the greatest extent. It is notable that chemotactic activity of CXCR4 is completely
456 extinguished at the CD4SP SM stage, despite continued CXCR4 expression, but not at the more mature
457 CD4SP and CD8SP stages, suggesting a thymocyte-intrinsic mechanism of diminished responsiveness to
458 CXCR4, similar to the lack of responsiveness to CCR7 ligands by this subset. It is possible that the lack of
459 CXCR4 activity in CD4SP SM cells may permit medullary entry, consistent with the need to release post-

460 positive selection thymocytes from binding to cTECs (Kadakia et al., 2019); however, DP CD3^{lo}CD69^{+} cells
461 enter the medulla just as efficiently as CD4SP SM cells despite continued CXCR4 responsiveness,
462 suggesting factors other than reduced CXCR4 activity likely enable medullary entry. The role for
463 increased CXCR4 activity in more mature SP thymocytes remains to be determined but could impact
464 thymocyte egress. Identifying intrinsic regulators of chemokine receptor responsiveness in different
465 thymocyte subsets will further our understanding of the complex mechanisms underlying the
466 orchestration of thymocyte movement and selection in the thymus.

467 A major outstanding question raised by our findings is whether the combinatorial and temporally
468 regulated changes in chemokine receptor expression on post-positive selection thymocytes drive
469 interactions with distinct APC subsets. Here we show that CCR7 ligands are expressed by mTECs, while
470 CCR4 ligands are expressed mainly by cDC2s and activated cDCs, with some expression by thymic B cells.
471 Thus, CCR7 activity may drive interactions with mTECs, possibly explaining why CCR7 is particularly
472 required for negative selection to TRAs, consistent with the finding that CCR7 deficiency results in
473 autoimmune infiltrates in endocrine organs, as occurs in Aire-deficient mice (Anderson et al., 2002;
474 Kurobe et al., 2006; Nitta et al., 2009). In contrast, CCR4 activity may promote interactions with and
475 tolerance to cDC2s, B cells, and activated cDCs, consistent with our finding that *Ccr4*$^{-/-}$ mice showed T
476 cell hyperplasia in secondary lymphoid organs and that *Ccr4*$^{-/-}$ T cells undergo increased proliferation to
477 LPS-activated splenic APCs. Recently, a subset of cDC2s has been shown to present circulating antigens
478 to induce negative selection, and another subset has been shown to traffic microbial antigens to the
479 thymus, impacting thymocyte selection (Atibalentja et al., 2009; Vollmann et al., 2021; Zegarra-Ruiz et
480 al., 2021). B cells also present self-antigens to induce thymocyte negative selection (Perera et al., 2016;
481 Yamano et al., 2015). While we find CCL22 is expressed predominantly in the medulla, and CCR4
482 promotes medullary accumulation of early- post positive selection DPs, our study does not rule out the
483 possibility that CCR4 could also enforce interactions between CCR4-responsive thymocytes and cortical

484 DCs expressing CCL22, which could contribute to cortical negative selection. This possibility is
485 particularly intriguing in light of the fact that DP $CD3^{lo}CD69^{+}$ and CD4SP SM cells respond to CCR4 ligands
486 and migrate both in the cortex and medulla. The finding that CCR4 and CCR7 cooperate to prevent
487 inflammation in the colon is unexpected and warrants further exploration. Whether the inflammatory
488 phenotypes observed reflect impaired central tolerance due to diminished interactions between
489 thymocytes and distinct thymic APCs and/or impaired peripheral tolerance remains to be determined.

490 Altogether, our findings suggest a layered process of central-tolerance induction in which CCR4 first
491 promotes interactions with DCs and B cells, driving self-tolerance to activated APCs, which may be
492 present in both the cortex and/or medulla. As thymocytes mature further, CCR7 is expressed and
493 becomes active, drawing the cells robustly into the medulla, where the partially tolerized repertoire can
494 be focused on tolerance induction to the sparse TRAs. One limitation of our current system is that ex
495 vivo live thymic slices are not equivalent to in situ thymi, as they lack circulation, for example. We note,
496 however, that short-term live thymic slice cultures have been widely used to investigate the
497 development, localization, migration, and positive and negative selection of thymocytes, as they have
498 been shown to faithfully reflect these in vivo processes, including confirming that CCR7 signaling induces
499 chemotaxis of mature thymocytes from the cortex into the medulla (Au-Yeung et al., 2014; Dzhagalov et
500 al., 2013; Ehrlich et al., 2009; Lancaster et al., 2019; Melichar et al., 2013; Ross et al., 2014). Because our
501 study measured differences in medullary accumulation of thymocytes that differed genetically only in
502 expression of CCR4 and/or CCR7, we attribute altered localization to the impact of these chemokine
503 receptors on thymocyte migration. However, we note the possibility that CCR4 and CCR7 could signal in
504 conjunction with survival cues, like cytokines, localized to different thymic microenvironments, which
505 could also impact survival of thymocytes in different regions. As thymocytes were imaged within a few
506 hours of entering slices, differential survival in the cortex and medulla due to cytokine cues is somewhat
507 less likely than differential migration. Multiple aspects of our revised model of thymocyte migration and

508 central tolerance, including the impact of CCR4 and CCR7 on interactions with distinct APCs during
509 tolerance induction and on selection of distinct TCR clones will be tested in future studies.

510 **Materials and Methods**

511 **Mice**

512 C57BL/6J (wild-type), B6.SJL-Ptprc^{a} PepC^{b} (CD45.1), C57BL/6-Tg(TcraTcrb)1100Mjb/J (OT-I), B6.Cg-
513 Tg(TcraTcrb)425Cbn/J (OT-II), B6(Cg)-Rag2$^{tm1.1Cgn}$/J (*Rag2*$^{-/-}$), B6.129P2(C)Ccr7^{tm1Rfo}r/J (*Ccr7*$^{-/-}$), B6.129S2-
514 H2$^{dlAb1-Ea}$/J (*MHCII*$^{-/-}$), B6.129P2-B2m^{tm1Unc}/DcrJ (*β2m*$^{-/-}$), C57BL/6-Tg(Nr4a1-EGFP/cre)820Khog/J
515 (Nur77^{GFP}) were purchased from the Jackson Laboratory. *Ccr4*$^{-/-}$(Chvatchko et al., 2000), pCX-EGFP
516 (Wright et al., 2001), and Rag2p-GFP (Boursalian et al., 2004) strains were generously provided by A.D.
517 Luster (Massachusetts General Hospital, Boston, MA), Irving L. Weissman (Stanford University, Stanford,
518 CA), and Ellen R. Richie (the University of Texas MD Anderson Center, Houston, Texas, United States),
519 respectively. *Ccr4*$^{-/-}$ *Ccr7*$^{-/-}$, OT-I *Rag2*$^{-/-}$, and OT-II *Rag2*$^{-/-}$ *MHCII*$^{-/-}$ strains were bred in house. Experiments
520 were performed using mice 4-8 weeks old, except for for autoimmune/inflammatory studies which were
521 carried out in older mice, as specified. All strains were bred and maintained under specific pathogen-
522 free conditions at the Animal Resources Center, the University of Texas at Austin, with procedure
523 approval from the Institutional Animal Care and Use Committee, the University of Texas at Austin.

524 **Flow cytometry**

525 5×10^{6} thymocytes were stained with fluorescently conjugated antibodies and a viability dye, and
526 incubated on ice for 30 minutes in the dark. Unless specified, for stains including anti-CCR7, cells were
527 instead incubated in a 37°C water bath for 45 minutes in the dark. Stained cells were washed and
528 resuspended in FACS Wash Buffer (PBS + 2% FBS (GemCell™, Gemini, CA, USA)) + 1µg/mL propidium
529 iodine (PI) if a fixable viability dye was not used. For cleaved caspase 3 stains, surface-stained cells were
530 fixed and permeabilized with the BD Cytofix/Cytoperm kit (BD, NJ, USA) according to manufacturer's

531 instructions prior to staining for anti-cleaved caspase 3 (Cell Signaling Technology, MA, USA). All flow
532 cytometry data were acquired on an LSR Fortessa flow cytometer (BD) and analyzed with FlowJo
533 ver.10.8.0 (BD).

534 **Transwell Chemotaxis assays**

535 Thymocyte chemotaxis assays were performed as previously described (Campbell et al., 1999). Briefly,
536 5×10^5 thymocytes were resuspended in 100µL RPMI 1640 (Gibco, MA, USA) + 10% Fetal Bovine Serum
537 (Gemini) and added to the top chamber of 5µm pore transwell tissue culture inserts (Corning, NY, USA)
538 in 24-well plates. The bottom chamber of the transwells contained recombinant mouse chemokines
539 CCL17, CCL22, CCL19, CCL21 (Peprotech, NJ, USA) or CCL25 (R&D Systems, MN, USA) at 100nM, 10nM
540 and 1nM, diluted in 500µL RPMI 1640 + 10% FBS. The plate was cultured at 37°C, 5% CO_2 for 2 hours.
541 Cells that migrated to the bottom wells, and 5×10^5 input cells, were analyzed and quantified by flow
542 cytometry. A standard number of 15µm polyester beads were added to each well to calculate the
543 absolute number of thymocytes that migrated. Migration percentages of each subset were calculated by
544 dividing the number of migrated cells of each subset by the number of cells of the same subset in the
545 input cell sample, and the migration index was calculated as the ratio of the migration percentage in
546 wells containing chemokine to the average migration percentage in wells without chemokine (Blank
547 wells).

548 ***Ex vivo* thymic slice preparation**

549 *Ex vivo* thymic slices were prepared as previous described (Lancaster & Ehrlich, 2017). Briefly, surgically
550 removed thymi were cleaned of residual connective tissue, and the two lobes were separated and
551 embedded in 4% low melting point agarose (Lonza, NJ, USA). 400µm thymic slices were generated by
552 slicing the trimmed agarose blocks on a VT 1000S vibratome (Leica, Germany) and kept on ice,
553 submerged in complete RPMI until addition of thymocytes. Slices were placed on 0.4µm cell culture

554 inserts (Millipore, MA, USA) in 35mm dishes containing 1mL complete RPMI (RPMI 1640 supplemented
555 with 1X GlutaMAX, 1mM Sodium Pyruvate, 1X Penicillin-Streptomycin-glutamine, 1X MEM Non-Essential
556 Amino Acid, and 50µM β-mercaptoethanol (All from Gibco), and 10% FBS (Gemini)).

557 **Synchronized positive selection thymic slice assays**

558 Synchronized positive selection assays were set up as previously described (Ross et al., 2014). Briefly, to
559 generate a source of pre-positive selection OT-I thymocytes, bone marrow from OT-I *Rag2*$^{-/-}$ hosts was
560 magnetically depleted of CD3^{+}, CD8^{+}, CD25^{+}, B220^{+}, Gr-1^{+}, CD11b^{+}, Ter119^{+} cells using Rat anti-mouse
561 antibodies (BioXcell, NH, USA) and Dynabeads™ sheep anti-rat IgG beads (Invitrogen, MA, USA)
562 according to manufacturer's recommendations, then 10^{7} cells were injected into lethally irradiated *β2m*$^{-}$
563 $^{/-}$ hosts. The bone marrow chimera recipients were maintained for 4-6 weeks before collecting OT-I pre-
564 selection thymocytes. For pre-positive selection OT-II thymocytes, OT-II *Rag2*$^{-/-}$ *MHCII*$^{-/-}$ mice were bred.
565 Thymic single cell suspensions from the OT-I *Rag2*$^{-/-}$ -> *β2m*$^{-/-}$ bone marrow chimeras or OT-II *Rag2*$^{-/-}$
566 *MHCII*$^{-/-}$ mice were isolated, stained in 5mL RPMI 1640 + 5µM CellTrace™ Violet (Invitrogen) for 30
567 minutes in the dark at 37°C, washed once with warm complete RPMI, resuspended in fresh, warm
568 complete RPMI, and kept in the dark at 37°C prior to slice addition. Prepared cells were overlaid on WT,
569 *β2m*$^{-/-}$, *MHCII*$^{-/-}$ or pCX-EGFP slices and incubated at 5% CO_2 37°C. Slices were gently washed at 3h with
570 warm complete RPMI in a dish to prevent further entry of new cells. At the indicated time points,
571 thymocytes were harvested by mechanical disruption of the slices for flow cytometry or intact slices
572 were imaged by 2-photon microscopy.

573 **2-photon imaging and analysis of thymic slices**

574 For imaging of purified thymocyte subsets, sorted cells from each host were centrifuged for collection,
575 then separately stained in RPMI 1640 with 5µM CellTracker™ Red CMTPX (Thermo Fisher Scientific, MA,
576 USA) or Indo-1 AM (eBioscience, CA, USA) for 30 minutes in 37°C water bath, away from light. Dye used

577 for each host was swapped between experiments to account for potential effect of dyes on cell viability
578 and mobility. For imaging of pre-positive selection thymocytes, whole thymus single cells were stained
579 in RPMI 1640 with 5µM CellTracker™ Red CMTPX in the same way. Stained cells were collected by
580 centrifugation and resuspended in fresh warm cRPMI, incubated for 30 minutes in 37°C water bath,
581 away from light. Prepared cells were collected by centrifugation, then washed 2 times with fresh warm
582 complete RPMI to remove dye residues, then laid onto pCX-EGFP slices, and incubated in 5% CO_2
583 incubator at 37°C for a minimum of 1 hour before 2-photon imaging.

584 For image and Video acquisition, thymic slices were secured to an imaging chamber (Harvard Apparatus,
585 MA, USA) perfused with heated DRPMI (Corning) + 2g/L sodium bicarbonate, 5mM HEPES (Sigma-
586 Aldrich, MA, USA) and 1.25mM $CaCl_2$, pH = 7.4, aerated with 95% O_2 + 5% CO_2 at flow rate of 100mL/h.
587 The imaging chamber is secured on a heated stage, and a temperature probe was inserted to monitor
588 and maintain the chamber temperature at 37°C. Images were acquired using an Ultima IV microscope
589 controlled by PrairieView software (V5.4, Bruker, MA, USA), with a 20X water immersion objective, NA =
590 1.0 (Olympus, Japan). Time-lapse Videos were acquired by a t-series of 60 rounds of 15s acquisition,
591 through 40µm depth at 5µm intervals. Samples were illuminated with a Mai Tai Ti:sapphire laser
592 (Spectra Physics) tuned to 865nm for simultaneous excitation of EGFP and CMTPX, and an additional
593 InSight Ti:sapphire laser (Spectra Physics, CA, USA) tuned to 730nm for excitation of Indo-1 AM, if
594 necessary. Emitted light was passed through 473/24, 525/50 and 605/70 band pass filters (Chroma, VT,
595 USA) to separate PMTs for detecting Indo-1 AM (low calcium), EGFP and CMTPX signals, respectively.

596 Captured images were analyzed using Imaris v9.7.2 (Bitplane, Switzerland). For medullary enrichment
597 analysis, medullary and cortical volumes were established by manually generating surface objects by
598 morphological distinction. Fluorescently labelled cells were identified using Spot tools from random
599 frames of each Video, and medullary or cortical cellular localization was determined by calculating the
600 spot's distance to the medullary surface object using the Spot distance to Surface function in ImarisXT.

601 Densities of cells within each region were calculated by dividing the number of cells in the respective
602 region by the volume of the surface object, and medullary-to-cortical ratio was calculated by dividing
603 the medullary density to the cortical density within the same Video, using Excel (Microsoft). For
604 thymocyte migration parameters, trajectory of thymocytes were established with the automated Spot
605 tracking feature within Imaris. Only trajectories with time span ≥ 3 minutes were included in the
606 analysis. Average track speed and straightness were generated by Imaris for analysis.

607 **cDNA preparation and qPCR**

608 FACS purified, frozen thymic APC subsets were thawed and lysed in TRIzol (Thermo Fisher), RNA was
609 extracted, and cDNA waw synthesized using the qScript cDNA Synthesis Kit (QuantaBio, MA, USA), per
610 manufacture's recommendations. qRT-PCR was performed using SYBR Green PCR Master Mix (Applied
611 Biosystems, MA, USA), on a ViiA 7 Real-Time PCR System (Applied Biosystems), using the following
612 primers: *Ccl17* Forward: 5'-AGT GGA GTG TTC CAG GGA TG-3', *Ccl17* Reverse: 5'-CCA ATC TGA TGG CCT
613 TCT TC-3', *Ccl19* Forward: 5'-GCT AAT GAT GCG GAA GAC TG-3', *Ccl19* Reverse: 5'-ACT CAC ATC GAC TCT
614 CTA GG-3', *Ccl21* Forward: 5'-GCA GTG ATG GAG GGG GTC AG-3', *Ccl21* Reverse: 5'-CGG GGT GAG AAC
615 AGG ATT GC-3', *Ccl22* Forward: 5'-AGG TCC CTA TGG TGC CAA TGT-3', *Ccl22* Reverse: 5'- CGG CAG GAT
616 TTT GAG GTC CA-3', β-actin Forward: 5'- CAC TGT CGA GTC GCG TCC A-3', β-actin Reverse: 5'- CAT CCA
617 TGG CGA ACT GGT GG-3'. ddCT Relative expression levels of target genes in each subset were quantified
618 by first normalizing to actin expression within each subset, then normalizing between subsets for
619 expression of target genes relative to a subset previously shown to express high levels of that gene. For
620 CCL17 and CCL22, expression levels were normalized to cDC2; For CCL19 and CCL21, expression levels
621 were normalized to $mTEC^{lo}$.

622 **Congenic TLR stimulation and co-culture experiment**

623 To activate APCs, congenic CD45.1 mouse spleen was isolated and red blood cells were lysed with RBC
624 lysis buffer (BioLegend, CA, USA). Leukocytes were then resuspended in complete RPMI with 1µg/mL
625 high molecular weight Poly(I:C), 1µg/mL low molecular weight Poly(I:C), 100ng/mL LPS, 500nM
626 ODN1826 (Invivogen, CA, USA), or without any TLR ligands, and incubated in 5% CO_2 incubator at 37°C
627 overnight. The next day, CD45.2 WT and *Ccr4*$^{-/-}$ CD4^{+} T cells were isolated from spleen by magnetically
628 depleting CD8^{+}, CD25^{+}, B220^{+}, CD11b^{+}, Gr-1^{+} and Ter119^{+} cells with corresponding rat anti-mouse
629 antibodies (BioXCell) and Dynabeads® sheep anti-rat IgG (Invitrogen), and resuspended in complete
630 RPMI. Stimulated CD45.1 splenocytes were washed three times with fresh complete RPMI. 2.5×10^{4} WT
631 or *Ccr4*$^{-/-}$ CD4^{+} purified T cells were plated with or without 1.25×10^{5} unstimulated or stimulated
632 splenocytes per well in complete RPMI in a 96-well, U-bottom plate. At Day 3 and Day 5, each well was
633 harvested and subjected to flow cytometry analysis. 15µm polyester beads of known quantities were
634 added to quantify cells in each sample.

635 **Immunofluorescent analyses of thymic and LNs cryosections and detection of autoantibodies**

636 To detect anti-nuclear autoantibodies in mouse serum, 7-µm cryosections were prepared from *Rag2*$^{-/-}$
637 kidneys (C57BL/6J background). Cryosections were fixed in acetone (-20°C for 20 minutes), rinsed 3X (2x
638 PBS rinses and 1x PBS with 0.1% Tween 20), blocked with 9% donkey serum (Jackson ImmunoResearch)
639 in PBS for 20 minutes and incubated with undiluted mouse serum from mice of the indicated genotypes
640 for 2 hours at room temperature. After washing, auto-antibodies were detected by staining with anti-
641 mouse IgG AF594 in PBS for 1 hour at room temperature. After washing, slides were incubated with
642 DAPI, washed, and coverslips were mounted in ProLong™ Gold Antifade reagent (ThermoFisher). For
643 CCL22 immunofluorescent staining and inguinal lymph node immunostaining, 7-µm cryosections were
644 prepared from the thymus of 1 month old C57BL/6J mice and from lymph nodes of 5–6-month-old mice,
645 respectively. All slides were fixed and stained as above. Thymus sections were stained with anti-CCL22

646 AF439, anti-CD11c-biotin and anti-CD31-APC overnight at room temperature. Inguinal lymph nodes
647 were stained with anti-CCL22, anti-CD11c -biotin, and anti-CD31 - APC overnight at room temperature.
648 For both, after washing, anti-goat-Dylight 488 and streptavidin Alexa Fluor 594 secondary antibodies
649 were incubated for 1 hour at room temperature. The DAPI nuclear stain was added and slides mounted
650 as above. Immunofluorescent images were acquired on a DMi8 microscope (Leica), using a 10x/0.4 NA
651 objective or a 20X/0.7NA objective. Stitched images were generated with LasX software (Leica). All
652 images were uniformly processed and converted into Tiffs using Fiji software (ImageJ),

653 **H&E staining and quantification**

654 Lacrimal glands, submandibular glands, colon, and liver were extracted from 6–8-month-old mice and
655 fixed in formalin (Fisherbrand) for 48 hours before storing in 70% ethanol. Organs were sent to the
656 Histology and Immunohistochemistry Laboratory at the University of Texas San Antonio for embedding,
657 sectioning, and staining. Spleen and mLNs were extracted and processed by the Histology and Tissue
658 Processing core at the University of Texas MD Anderson Cancer Center Science Park (Smithville, TX).
659 Histological analysis of spleen, inguinal lymph nodes, liver and colon were done by a veterinary
660 pathologist, while infiltrates in lacrimal and submandibular glands stains were analyzed in-house, as in
661 previously described (Lieberman et al., 2015). Briefly, we scored foci composed of at least 50
662 mononuclear cells. In the cases where multiple foci coalesced, we assigned those foci a score value of 3
663 for statistical analysis. The number of inflammatory foci per 10 mm^2 was calculated by counting the
664 total number of foci by standard light microscopy using a 10 × objective and dividing that by the surface
665 area of sections measured by Fiji software. Colon sections were scored for mucosal changes such as
666 hyperplasia and architectural distortion, inflammation severity, and the percentage of the tissue
667 affected as described previously (Hale et al., 2005), but with a single score that reflected the entire
668 segment examined (total possible scores ranged from 0 – 15).

669 **Statistical analysis**

670 All statistical analysis was conducted using Graphpad PRISM v9.8 (Graphpad Software, CA, USA), with
671 the corresponding statistical tests and multiple comparison corrections listed in the figure legends.

672

673 **Acknowledgements:** The authors thank the Animal Resource Center staff at the University of Texas at
674 Austin for assistance with mouse maintenance, Dr. Jessica Lancaster for assistance with 2-photon
675 microscopy training, Richard Salinas at the Center for Biomedical Research Support, and Dr. Ellen Richie
676 for providing advice. Graphical illustrations were created with Biorender.com. This research was
677 supported by a grant from the National Institutes of Health R01AI104870 to L.I.R.E.

678 **Author contributions:** Y.L. and P.G.T. designed and conducted experiments, analyzed data, and wrote
679 and edited the manuscript. J.S. and H.J.S. conducted experiments. L.P.H carried out histologic analyses
680 and edited the manuscript. L.I.R.E. designed experiments, analyzed data, and edited the manuscript.

681 **Competing Interests statement:** The authors have no conflicts of interest to declare.

682

683 **References**

684 Abramson, J., & Anderson, G. (2017). Thymic Epithelial Cells. *Annu Rev Immunol*, *35*(1), 85-118.
685 https://doi.org/10.1146/annurev-immunol-051116-052320
686 Alam, A., Braun, M. Y., Hartgers, F., Lesage, S., Cohen, L., Hugo, P., Denis, F., & Sékaly, R.-P. (1997).
687 Specific Activation of the Cysteine Protease CPP32 during the Negative Selection of T Cells in the
688 Thymus. *Journal of Experimental Medicine*, *186*(9), 1503-1512.
689 https://doi.org/10.1084/jem.186.9.1503
690 Anderson, M. S., & Su, M. A. (2016). AIRE expands: new roles in immune tolerance and beyond. *Nat Rev*
691 *Immunol*, *16*(4), 247-258. https://doi.org/10.1038/nri.2016.9
692 Anderson, M. S., Venanzi, E. S., Klein, L., Chen, Z., Berzins, S. P., Turley, S. J., von Boehmer, H., Bronson,
693 R., Dierich, A., Benoist, C., & Mathis, D. (2002). Projection of an immunological self shadow
694 within the thymus by the aire protein. *Science*, *298*(5597), 1395-1401.
695 https://doi.org/10.1126/science.1075958
696 Ardouin, L., Luche, H., Chelbi, R., Carpentier, S., Shawket, A., Montanana Sanchis, F., Santa Maria, C.,
697 Grenot, P., Alexandre, Y., Gregoire, C., Fries, A., Vu Manh, T. P., Tamoutounour, S., Crozat, K.,
698 Tomasello, E., Jorquera, A., Fossum, E., Bogen, B., Azukizawa, H., . . . Malissen, B. (2016). Broad
699 and Largely Concordant Molecular Changes Characterize Tolerogenic and Immunogenic
700 Dendritic Cell Maturation in Thymus and Periphery. *Immunity*, *45*(2), 305-318.
701 https://doi.org/10.1016/j.immuni.2016.07.019
702 Atibalentja, D. F., Byersdorfer, C. A., & Unanue, E. R. (2009). Thymus-blood protein interactions are
703 highly effective in negative selection and regulatory T cell induction. *J Immunol*, *183*(12), 7909-
704 7918. https://doi.org/10.4049/jimmunol.0902632
705 Au-Yeung, B. B., Melichar, H. J., Ross, J. O., Cheng, D. A., Zikherman, J., Shokat, K. M., Robey, E. A., &
706 Weiss, A. (2014). Quantitative and temporal requirements revealed for Zap70 catalytic activity
707 during T cell development. *Nat Immunol*, *15*(7), 687-694. https://doi.org/10.1038/ni.2918
708 Azzam, H. S., Grinberg, A., Lui, K., Shen, H., Shores, E. W., & Love, P. E. (1998). CD5 expression is
709 developmentally regulated by T cell receptor (TCR) signals and TCR avidity. *J Exp Med*, *188*(12),
710 2301-2311. https://doi.org/10.1084/jem.188.12.2301
711 Bendelac, A., Killeen, N., Littman, D. R., & Schwartz, R. H. (1994). A subset of CD4+ thymocytes selected
712 by MHC class I molecules. *Science*, *263*(5154), 1774-1778.
713 https://doi.org/10.1126/science.7907820
714 Bleul, C. C., & Boehm, T. (2000). Chemokines define distinct microenvironments in the developing
715 thymus. *Eur J Immunol*, *30*(12), 3371-3379. https://doi.org/10.1002/1521-
716 4141(2000012)30:12<3371::AID-IMMU3371>3.0.CO;2-L
717 Bonasio, R., Scimone, M. L., Schaerli, P., Grabie, N., Lichtman, A. H., & von Andrian, U. H. (2006). Clonal
718 deletion of thymocytes by circulating dendritic cells homing to the thymus. *Nat Immunol*, *7*(10),
719 1092-1100. https://doi.org/10.1038/ni1385
720 Bornstein, C., Nevo, S., Giladi, A., Kadouri, N., Pouzolles, M., Gerbe, F., David, E., Machado, A., Chuprin,
721 A., Toth, B., Goldberg, O., Itzkovitz, S., Taylor, N., Jay, P., Zimmermann, V. S., Abramson, J., &
722 Amit, I. (2018). Single-cell mapping of the thymic stroma identifies IL-25-producing tuft epithelial
723 cells. *Nature*, *559*(7715), 622-626. https://doi.org/10.1038/s41586-018-0346-1
724 Boursalian, T. E., Golob, J., Soper, D. M., Cooper, C. J., & Fink, P. J. (2004). Continued maturation of
725 thymic emigrants in the periphery. *Nat Immunol*, *5*(4), 418-425. https://doi.org/10.1038/ni1049
726 Breed, E. R., Watanabe, M., & Hogquist, K. A. (2019). Measuring Thymic Clonal Deletion at the
727 Population Level. *J Immunol*, *202*(11), 3226-3233. https://doi.org/10.4049/jimmunol.1900191
728 Brennecke, P., Reyes, A., Pinto, S., Rattay, K., Nguyen, M., Kuchler, R., Huber, W., Kyewski, B., &
729 Steinmetz, L. M. (2015). Single-cell transcriptome analysis reveals coordinated ectopic gene-

730 expression patterns in medullary thymic epithelial cells. *Nat Immunol*, *16*(9), 933-941.
731 https://doi.org/10.1038/ni.3246
732 Britschgi, M. R., Link, A., Lissandrin, T. K. A., & Luther, S. A. (2008). Dynamic Modulation of CCR7
733 Expression and Function on Naive T Lymphocytes In Vivo1. *The Journal of Immunology*, *181*(11),
734 7681-7688. https://doi.org/10.4049/jimmunol.181.11.7681
735 Brugnera, E., Bhandoola, A., Cibotti, R., Yu, Q., Guinter, T. I., Yamashita, Y., Sharrow, S. O., & Singer, A.
736 (2000). Coreceptor reversal in the thymus: signaled CD4+8+ thymocytes initially terminate CD8
737 transcription even when differentiating into CD8+ T cells. *Immunity*, *13*(1), 59-71.
738 https://doi.org/10.1016/s1074-7613(00)00008-x
739 Campbell, J. J., Pan, J., & Butcher, E. C. (1999). Cutting edge: developmental switches in chemokine
740 responses during T cell maturation. *J Immunol*, *163*(5), 2353-2357.
741 https://doi.org/ji_v163n5p2353 [pii]
742 Cepeda, S., Cantu, C., Orozco, S., Xiao, Y., Brown, Z., Semwal, M. K., Venables, T., Anderson, M. S., &
743 Griffith, A. V. (2018). Age-Associated Decline in Thymic B Cell Expression of Aire and Aire-
744 Dependent Self-Antigens. *Cell Rep*, *22*(5), 1276-1287.
745 https://doi.org/10.1016/j.celrep.2018.01.015
746 Chvatchko, Y., Hoogewerf, A. J., Meyer, A., Alouani, S., Juillard, P., Buser, R., Conquet, F., Proudfoot, A. E.
747 I., Wells, T. N. C., & Power, C. A. (2000). A Key Role for Cc Chemokine Receptor 4 in
748 Lipopolysaccharide-Induced Endotoxic Shock. *Journal of Experimental Medicine*, *191*(10), 1755-
749 1764. https://doi.org/10.1084/jem.191.10.1755
750 Cowan, J. E., McCarthy, N. I., Parnell, S. M., White, A. J., Bacon, A., Serge, A., Irla, M., Lane, P. J.,
751 Jenkinson, E. J., Jenkinson, W. E., & Anderson, G. (2014). Differential requirement for CCR4 and
752 CCR7 during the development of innate and adaptive alphabetaT cells in the adult thymus. *J*
753 *Immunol*, *193*(3), 1204-1212. https://doi.org/10.4049/jimmunol.1400993
754 Daley, S. R., Hu, D. Y., & Goodnow, C. C. (2013). Helios marks strongly autoreactive CD4+ T cells in two
755 major waves of thymic deletion distinguished by induction of PD-1 or NF-kappaB. *J Exp Med*,
756 *210*(2), 269-285. https://doi.org/10.1084/jem.20121458
757 DeVoss, J., Hou, Y., Johannes, K., Lu, W., Liou, G. I., Rinn, J., Chang, H., Caspi, R. R., Fong, L., & Anderson,
758 M. S. (2006). Spontaneous autoimmunity prevented by thymic expression of a single self-
759 antigen. *J Exp Med*, *203*(12), 2727-2735. https://doi.org/10.1084/jem.20061864
760 Dzhagalov, I. L., Chen, K. G., Herzmark, P., & Robey, E. A. (2013). Elimination of self-reactive T cells in the
761 thymus: a timeline for negative selection. *PLoS Biol*, *11*(5), e1001566.
762 https://doi.org/10.1371/journal.pbio.1001566
763 Ehrlich, L. I., Oh, D. Y., Weissman, I. L., & Lewis, R. S. (2009). Differential contribution of chemotaxis and
764 substrate restriction to segregation of immature and mature thymocytes. *Immunity*, *31*(6), 986-
765 998. https://doi.org/10.1016/j.immuni.2009.09.020
766 Control of Migration during Intrathymic T Cell Development, 1 Encyclopedia of Immunobiology 249-262
767 (Elsevier 2016).
768 Finnish-German, A. C. (1997). An autoimmune disease, APECED, caused by mutations in a novel gene
769 featuring two PHD-type zinc-finger domains. *Nat Genet*, *17*(4), 399-403.
770 https://doi.org/10.1038/ng1297-399
771 Fu, G., Vallee, S., Rybakin, V., McGuire, M. V., Ampudia, J., Brockmeyer, C., Salek, M., Fallen, P. R.,
772 Hoerter, J. A., Munshi, A., Huang, Y. H., Hu, J., Fox, H. S., Sauer, K., Acuto, O., & Gascoigne, N. R.
773 (2009). Themis controls thymocyte selection through regulation of T cell antigen receptor-
774 mediated signaling. *Nat Immunol*, *10*(8), 848-856. https://doi.org/10.1038/ni.1766
775 Hale, L. P., Greer, P. K., Trinh, C. T., & Gottfried, M. R. (2005). Treatment with oral bromelain decreases
776 colonic inflammation in the IL-10-deficient murine model of inflammatory bowel disease.

777 *Clinical Immunology*, *116*(2), 135-142.
778 https://doi.org/https://doi.org/10.1016/j.clim.2005.04.011
779 Hawiger, D., Masilamani, R. F., Bettelli, E., Kuchroo, V. K., & Nussenzweig, M. C. (2004). Immunological
780 unresponsiveness characterized by increased expression of CD5 on peripheral T cells induced by
781 dendritic cells in vivo. *Immunity*, *20*(6), 695-705. https://doi.org/10.1016/j.immuni.2004.05.002
782 Hu, D. Y., Yap, J. Y., Wirasinha, R. C., Howard, D. R., Goodnow, C. C., & Daley, S. R. (2016). A timeline
783 demarcating two waves of clonal deletion and Foxp3 upregulation during thymocyte
784 development. *Immunol Cell Biol*, *94*(4), 357-366. https://doi.org/10.1038/icb.2015.95
785 Hu, Z., Lancaster, J. N., & Ehrlich, L. I. (2015). The Contribution of Chemokines and Migration to the
786 Induction of Central Tolerance in the Thymus. *Front Immunol*, *6*, 398.
787 https://doi.org/10.3389/fimmu.2015.00398
788 Hu, Z., Lancaster, J. N., Sasiponganan, C., & Ehrlich, L. I. (2015). CCR4 promotes medullary entry and
789 thymocyte-dendritic cell interactions required for central tolerance. *J Exp Med*, *212*(11), 1947-
790 1965. https://doi.org/10.1084/jem.20150178
791 Hu, Z., Li, Y., Van Nieuwenhuijze, A., Selden, H. J., Jarrett, A. M., Sorace, A. G., Yankeelov, T. E., Liston, A.,
792 & Ehrlich, L. I. R. (2017). CCR7 Modulates the Generation of Thymic Regulatory T Cells by
793 Altering the Composition of the Thymic Dendritic Cell Compartment. *Cell Rep*, *21*(1), 168-180.
794 https://doi.org/10.1016/j.celrep.2017.09.016
795 Kadakia, T., Tai, X., Kruhlak, M., Wisniewski, J., Hwang, I. Y., Roy, S., Guinter, T. I., Alag, A., Kehrl, J. H.,
796 Zhuang, Y., & Singer, A. (2019). E-protein-regulated expression of CXCR4 adheres preselection
797 thymocytes to the thymic cortex. *J Exp Med*, *216*(8), 1749-1761.
798 https://doi.org/10.1084/jem.20182285
799 Ki, S., Park, D., Selden, H. J., Seita, J., Chung, H., Kim, J., Iyer, V. R., & Ehrlich, L. I. R. (2014). Global
800 transcriptional profiling reveals distinct functions of thymic stromal subsets and age-related
801 changes during thymic involution. *Cell Rep*, *9*(1), 402-415.
802 https://doi.org/10.1016/j.celrep.2014.08.070
803 Klein, L., Kyewski, B., Allen, P. M., & Hogquist, K. A. (2014). Positive and negative selection of the T cell
804 repertoire: what thymocytes see (and don't see). *Nat Rev Immunol*, *14*(6), 377-391.
805 https://doi.org/10.1038/nri3667
806 Klein, L., Robey, E. A., & Hsieh, C. S. (2019). Central CD4(+) T cell tolerance: deletion versus regulatory T
807 cell differentiation. *Nat Rev Immunol*, *19*(1), 7-18. https://doi.org/10.1038/s41577-018-0083-6
808 Koble, C., & Kyewski, B. (2009). The thymic medulla: a unique microenvironment for intercellular self-
809 antigen transfer. *J Exp Med*, *206*(7), 1505-1513. https://doi.org/10.1084/jem.20082449
810 Kozai, M., Kubo, Y., Katakai, T., Kondo, H., Kiyonari, H., Schaeuble, K., Luther, S. A., Ishimaru, N.,
811 Ohigashi, I., & Takahama, Y. (2017). Essential role of CCL21 in establishment of central self-
812 tolerance in T cells. *J Exp Med*, *214*(7), 1925-1935. https://doi.org/10.1084/jem.20161864
813 Kurobe, H., Liu, C., Ueno, T., Saito, F., Ohigashi, I., Seach, N., Arakaki, R., Hayashi, Y., Kitagawa, T., Lipp,
814 M., Boyd, R. L., & Takahama, Y. (2006). CCR7-dependent cortex-to-medulla migration of
815 positively selected thymocytes is essential for establishing central tolerance. *Immunity*, *24*(2),
816 165-177. https://doi.org/10.1016/j.immuni.2005.12.011
817 Lancaster, J. N., & Ehrlich, L. I. R. (2017). Analysis of Thymocyte Migration, Cellular Interactions, and
818 Activation by Multiphoton Fluorescence Microscopy of Live Thymic Slices. In G. E. Rainger & H.
819 M. McGettrick (Eds.), *T-Cell Trafficking: Methods and Protocols* (pp. 9-25). Springer New York.
820 https://doi.org/10.1007/978-1-4939-6931-9_2
821 Lancaster, J. N., Li, Y., & Ehrlich, L. I. R. (2018). Chemokine-Mediated Choreography of Thymocyte
822 Development and Selection. *Trends Immunol*, *39*(2), 86-98.
823 https://doi.org/10.1016/j.it.2017.10.007

824 Lancaster, J. N., Thyagarajan, H. M., Srinivasan, J., Li, Y., Hu, Z., & Ehrlich, L. I. R. (2019). Live-cell imaging
825 reveals the relative contributions of antigen-presenting cell subsets to thymic central tolerance.
826 *Nat Commun*, *10*(1), 2220. https://doi.org/10.1038/s41467-019-09727-4
827 Liu, B., Lin, Y., Yan, J., Yao, J., Liu, D., Ma, W., Wang, J., Liu, W., Wang, C., Zhang, L., & Qi, H. (2021).
828 Affinity-coupled CCL22 promotes positive selection in germinal centres. *Nature*, *592*(7852), 133-
829 137. https://doi.org/10.1038/s41586-021-03239-2
830 Lutes, L. K., Steier, Z., McIntyre, L. L., Pandey, S., Kaminski, J., Hoover, A. R., Ariotti, S., Streets, A., Yosef,
831 N., & Robey, E. A. (2021). T cell self-reactivity during thymic development dictates the timing of
832 positive selection. *eLife*, *10*, 1-28. https://doi.org/10.7554/eLife.65435
833 Marchetti, M. C., Di Marco, B., Cifone, G., Migliorati, G., & Riccardi, C. (2003). Dexamethasone-induced
834 apoptosis of thymocytes: role of glucocorticoid receptor-associated Src kinase and caspase-8
835 activation. *Blood*, *101*(2), 585-593. https://doi.org/10.1182/blood-2002-06-1779
836 Mathis, D., & Benoist, C. (2007). A decade of AIRE. *Nat Rev Immunol*, *7*(8), 645-650.
837 https://doi.org/10.1038/nri2136
838 McCaughtry, T. M., Baldwin, T. A., Wilken, M. S., & Hogquist, K. A. (2008). Clonal deletion of thymocytes
839 can occur in the cortex with no involvement of the medulla. *J Exp Med*, *205*(11), 2575-2584.
840 https://doi.org/10.1084/jem.20080866
841 McCaughtry, T. M., Wilken, M. S., & Hogquist, K. A. (2007). Thymic emigration revisited. *J Exp Med*,
842 *204*(11), 2513-2520. https://doi.org/10.1084/jem.20070601
843 Melichar, H. J., Ross, J. O., Herzmark, P., Hogquist, K. A., & Robey, E. A. (2013). Distinct temporal
844 patterns of T cell receptor signaling during positive versus negative selection in situ. *Sci Signal*,
845 *6*(297), ra92. https://doi.org/10.1126/scisignal.2004400
846 Meredith, M., Zemmour, D., Mathis, D., & Benoist, C. (2015). Aire controls gene expression in the thymic
847 epithelium with ordered stochasticity. *Nat Immunol*, *16*(9), 942-949.
848 https://doi.org/10.1038/ni.3247
849 Misslitz, A., Pabst, O., Hintzen, G., Ohl, L., Kremmer, E., Petrie, H. T., & Forster, R. (2004). Thymic T cell
850 development and progenitor localization depend on CCR7. *J Exp Med*, *200*(4), 481-491.
851 https://doi.org/10.1084/jem.20040383
852 Nagamine, K., Peterson, P., Scott, H. S., Kudoh, J., Minoshima, S., Heino, M., Krohn, K. J., Lalioti, M. D.,
853 Mullis, P. E., Antonarakis, S. E., Kawasaki, K., Asakawa, S., Ito, F., & Shimizu, N. (1997). Positional
854 cloning of the APECED gene. *Nat Genet*, *17*(4), 393-398. https://doi.org/10.1038/ng1297-393
855 Nitta, T., Nitta, S., Lei, Y., Lipp, M., & Takahama, Y. (2009). CCR7-mediated migration of developing
856 thymocytes to the medulla is essential for negative selection to tissue-restricted antigens. *Proc*
857 *Natl Acad Sci U S A*, *106*(40), 17129-17133. https://doi.org/10.1073/pnas.0906956106
858 Oh, J., Wu, N., Barczak, A. J., Barbeau, R., Erle, D. J., & Shin, J. S. (2018). CD40 Mediates Maturation of
859 Thymic Dendritic Cells Driven by Self-Reactive CD4(+) Thymocytes and Supports Development of
860 Natural Regulatory T Cells. *J Immunol*, *200*(4), 1399-1412.
861 https://doi.org/10.4049/jimmunol.1700768
862 Perera, J., Zheng, Z., Li, S., Gudjonson, H., Kalinina, O., Benichou, J. I. C., Block, K. E., Louzoun, Y., Yin, D.,
863 Chong, A. S., Dinner, A. R., Weigert, M., & Huang, H. (2016). Self-Antigen-Driven Thymic B Cell
864 Class Switching Promotes T Cell Central Tolerance. *Cell Rep*, *17*(2), 387-398.
865 https://doi.org/10.1016/j.celrep.2016.09.011
866 Persaud, S. P., Parker, C. R., Lo, W. L., Weber, K. S., & Allen, P. M. (2014). Intrinsic CD4+ T cell sensitivity
867 and response to a pathogen are set and sustained by avidity for thymic and peripheral
868 complexes of self peptide and MHC. *Nat Immunol*, *15*(3), 266-274.
869 https://doi.org/10.1038/ni.2822

870 Petrie, H. T., & Zuniga-Pflucker, J. C. (2007). Zoned out: functional mapping of stromal signaling
871 microenvironments in the thymus. *Annu Rev Immunol*, *25*, 649-679.
872 https://doi.org/10.1146/annurev.immunol.23.021704.115715
873 Ross, J. O., Melichar, H. J., Au-Yeung, B. B., Herzmark, P., Weiss, A., & Robey, E. A. (2014). Distinct phases
874 in the positive selection of CD8+ T cells distinguished by intrathymic migration and T-cell
875 receptor signaling patterns. *Proc Natl Acad Sci U S A*, *111*(25), E2550-2558.
876 https://doi.org/10.1073/pnas.1408482111
877 Ruscher, R., Kummer, R. L., Lee, Y. J., Jameson, S. C., & Hogquist, K. A. (2017). CD8alphaalpha
878 intraepithelial lymphocytes arise from two main thymic precursors. *Nat Immunol*, *18*(7), 771-
879 779. https://doi.org/10.1038/ni.3751
880 Sansom, S. N., Shikama-Dorn, N., Zhanybekova, S., Nusspaumer, G., Macaulay, I. C., Deadman, M. E.,
881 Heger, A., Ponting, C. P., & Hollander, G. A. (2014). Population and single-cell genomics reveal
882 the Aire dependency, relief from Polycomb silencing, and distribution of self-antigen expression
883 in thymic epithelia. *Genome Res*, *24*(12), 1918-1931. https://doi.org/10.1101/gr.171645.113
884 Sinclair, C., Bains, I., Yates, A. J., & Seddon, B. (2013). Asymmetric thymocyte death underlies the
885 CD4:CD8 T-cell ratio in the adaptive immune system. *Proc Natl Acad Sci U S A*, *110*(31), E2905-
886 2914. https://doi.org/10.1073/pnas.1304859110
887 Stritesky, G. L., Xing, Y., Erickson, J. R., Kalekar, L. A., Wang, X., Mueller, D. L., Jameson, S. C., & Hogquist,
888 K. A. (2013). Murine thymic selection quantified using a unique method to capture deleted T
889 cells. *Proc Natl Acad Sci U S A*, *110*(12), 4679-4684. https://doi.org/10.1073/pnas.1217532110
890 Ueno, T., Hara, K., Willis, M. S., Malin, M. A., Hopken, U. E., Gray, D. H., Matsushima, K., Lipp, M.,
891 Springer, T. A., Boyd, R. L., Yoshie, O., & Takahama, Y. (2002). Role for CCR7 ligands in the
892 emigration of newly generated T lymphocytes from the neonatal thymus. *Immunity*, *16*(2), 205-
893 218. https://doi.org/10.1016/s1074-7613(02)00267-4
894 Ueno, T., Saito, F., Gray, D. H., Kuse, S., Hieshima, K., Nakano, H., Kakiuchi, T., Lipp, M., Boyd, R. L., &
895 Takahama, Y. (2004). CCR7 signals are essential for cortex-medulla migration of developing
896 thymocytes. *J Exp Med*, *200*(4), 493-505. https://doi.org/10.1084/jem.20040643
897 Vollmann, E. H., Rattay, K., Barreiro, O., Thiriot, A., Fuhlbrigge, R. A., Vrbanac, V., Kim, K. W., Jung, S.,
898 Tager, A. M., & von Andrian, U. H. (2021). Specialized transendothelial dendritic cells mediate
899 thymic T-cell selection against blood-borne macromolecules. *Nat Commun*, *12*(1), 6230.
900 https://doi.org/10.1038/s41467-021-26446-x
901 Wright, D. E., Cheshier, S. H., Wagers, A. J., Randall, T. D., Christensen, J. L., & Weissman, I. L. (2001).
902 Cyclophosphamide/granulocyte colony-stimulating factor causes selective mobilization of bone
903 marrow hematopoietic stem cells into the blood after M phase of the cell cycle. *Blood*, *97*(8),
904 2278-2285. https://doi.org/10.1182/blood.v97.8.2278
905 Xing, Y., Wang, X., Jameson, S. C., & Hogquist, K. A. (2016). Late stages of T cell maturation in the thymus
906 involve NF-kappaB and tonic type I interferon signaling. *Nat Immunol*, *17*(5), 565-573.
907 https://doi.org/10.1038/ni.3419
908 Yamano, T., Nedjic, J., Hinterberger, M., Steinert, M., Koser, S., Pinto, S., Gerdes, N., Lutgens, E.,
909 Ishimaru, N., Busslinger, M., Brors, B., Kyewski, B., & Klein, L. (2015). Thymic B Cells Are Licensed
910 to Present Self Antigens for Central T Cell Tolerance Induction. *Immunity*, *42*(6), 1048-1061.
911 https://doi.org/10.1016/j.immuni.2015.05.013
912 Zegarra-Ruiz, D. F., Kim, D. V., Norwood, K., Kim, M., Wu, W. H., Saldana-Morales, F. B., Hill, A. A.,
913 Majumdar, S., Orozco, S., Bell, R., Round, J. L., Longman, R. S., Egawa, T., Bettini, M. L., & Diehl,
914 G. E. (2021). Thymic development of gut-microbiota-specific T cells. *Nature*, *594*(7863), 413-417.
915 https://doi.org/10.1038/s41586-021-03531-1

916

Figures and Legends

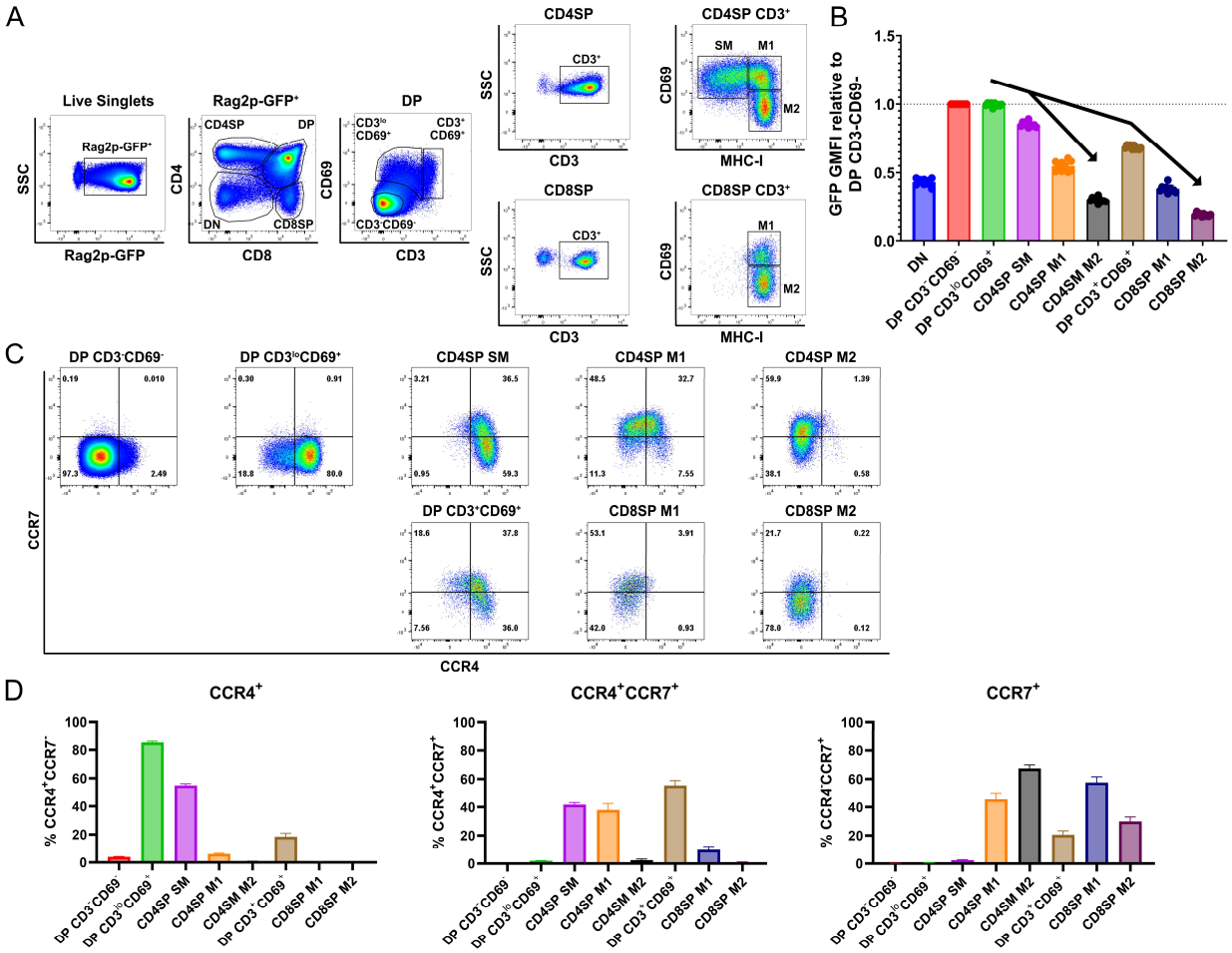

Figure 1. CCR4 and CCR7 are expressed by immature and mature subsets of post-positive selection thymocytes, respectively.

A) Flow cytometry gating scheme to delineate thymocyte subsets in Rag2p-GFP mice. Post-positive selection DP ($CD3^{lo}CD69^{+}$ and $CD3^{+}CD69^{+}$), CD4SP (SM, M1, and M2), and CD8SP (M1 and M2) subsets are annotated. **B)** Relative Rag2p-GFP Geometric Mean Fluorescent Intensity (GMFI) of each subset normalized to pre-positive selection DP $CD3^{-}CD69^{-}$ cells. Individual data points represent average GFP GMFI of the indicated subset from each mouse. **C)** Representative flow cytometry plots showing CCR4 and CCR7 expression by post-positive selection thymocyte subsets. **D)** Quantification of the percentage of cells of the indicated subset that express CCR4, CCR7, or both chemokine receptors. For B) and D), data were compiled from 4 independent experiments (Mean ± SEM; N=10 mice).

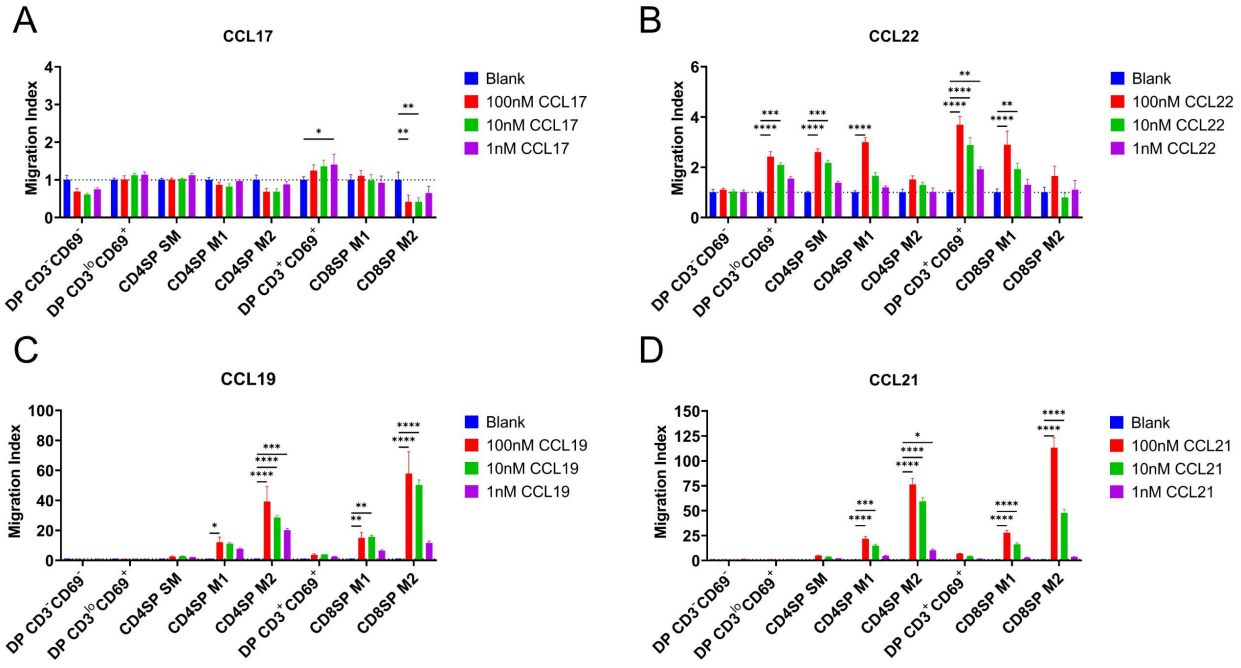

Figure 2. **CCR4 and CCR7 promote chemotaxis of immature and mature post-positive selection thymocyte subsets, respectively.**

A-D) Transwell assays were used to quantify chemotaxis of thymocyte subsets to the indicated concentrations of the CCR4 ligands CCL17 (A) and CCL22 (B) and the CCR7 ligands CCL19 (C) and CCL21 (D). Migration indexes were calculated as the frequencies of input cells of each subset that migrated towards the chemokine relative to the frequencies of input cells that migrated in the absence of chemokine (Blank). Data were compiled from 3 independent experiments with triplicate wells per assay. 2-way ANOVA with Dunnett's multiple comparison correction were used for statistical analysis. (Mean ± SEM; *: $p<0.05$, **: $p<0.01$, ***: $p<0.001$, ****: $p<0.0001$)

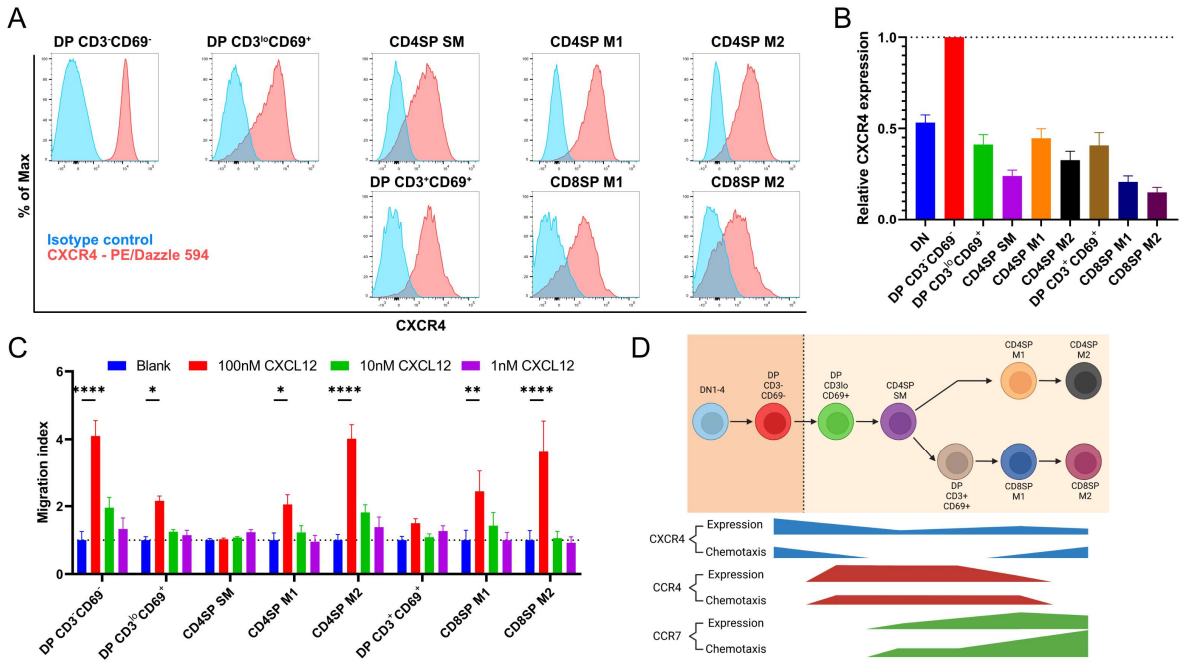

Figure 3. Persistent CXCR4 expression was detected on post-positive selection thymocytes, and CXCR4 activity declines only in intermediate subsets.

A) Representative flow cytometry plots showing CXCR4 surface expression by the indicated thymocyte subsets, compared to isotype control stains. **B)** Quantification of relative GMFI of CXCR4 for the indicated thymocyte subsets. (Mean ± SEM; N=10) **C)** Transwell assays were used to quantify chemotaxis of thymocyte subsets to the indicated concentrations of CXCL12. Migration indexes were calculated as the frequencies of input cells of each subset that migrated towards the chemokine relative to the frequencies of input cells that migrated in the absence of chemokine (Blank). Data were compiled from 3 independent experiments with triplicate wells per assay. 2-way ANOVA with Dunnett's multiple comparison correction were used for statistical analysis. (Mean ± SEM; *: $p<0.05$, **: $p<0.01$, ***: $p<0.001$, ****: $p<0.0001$) **D)** Graphical summary showing relative expression and chemotactic activity of CXCR4, CCR4 and CCR7 on post-positive selection thymocyte subsets based on data in Figures 1-3.

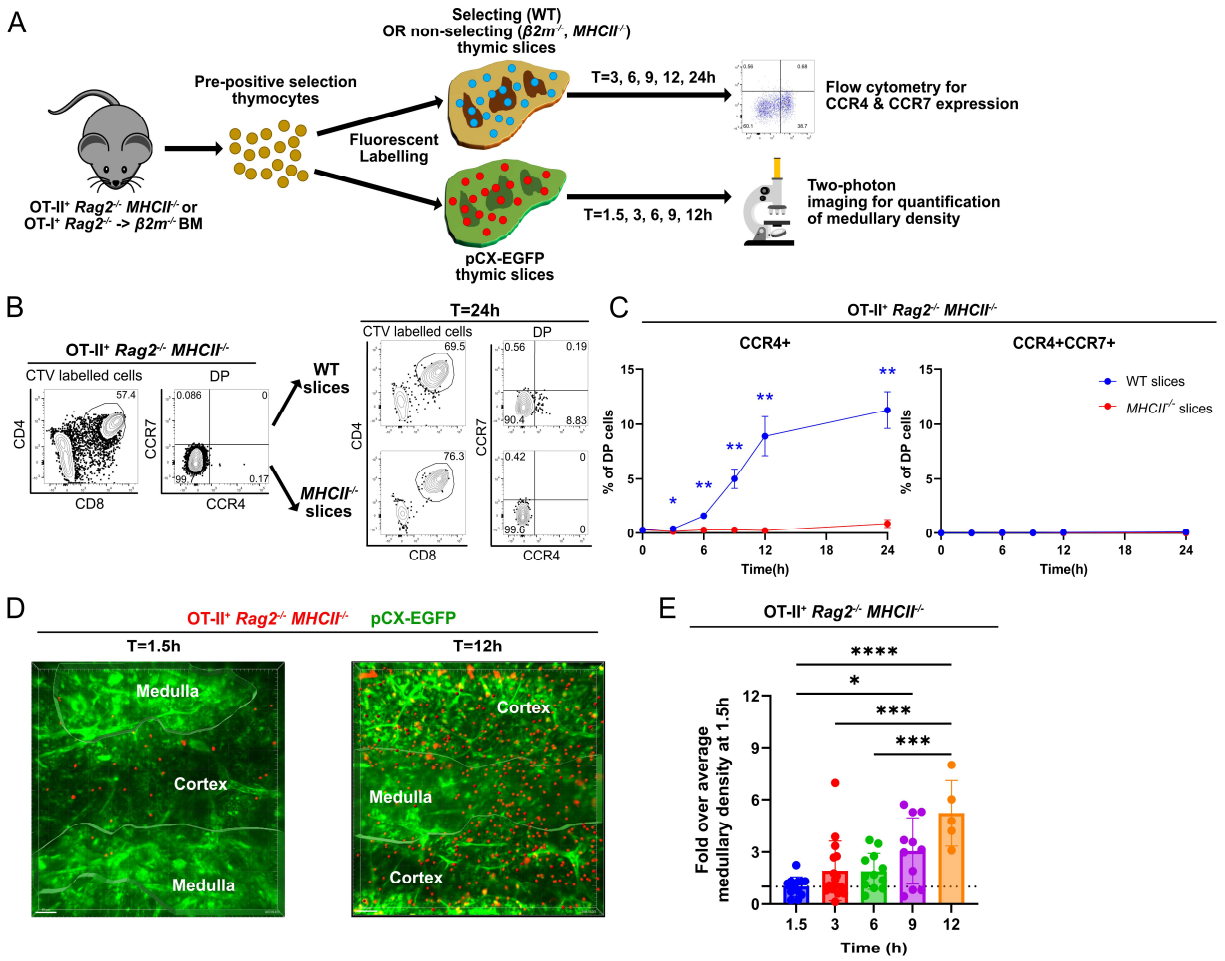

Figure 4. Rapid upregulation of CCR4 following positive selection of OT-II thymocytes correlates with medullary entry.

A) Experimental schematic of synchronized thymic slice positive selection assay to determine timing of CCR4 and CCR7 expression by flow cytometry and medullary entry by 2-photon microscopy. **B)** Representative flow cytometry plots showing CCR4 and CCR7 expression of OT-II^{+} *Rag2*$^{-/-}$ *MHCII*$^{-/-}$ thymocytes added to thymic slices (left) and analyzed 24h after incubation in WT or *MHCII*$^{-/-}$ slices, as indicated (right). **C)** Percentages of CCR4^{+} and CCR4^{+}CCR7^{+} OT-II^{+} thymocytes in thymic slices of the indicated genotypes at the indicated time points. Data were compiled from 3 experiments with triplicate slices each. Mixed-effect analysis with Šídák's multiple comparison correction was used for statistical analysis. (Mean ± SEM; *: p<0.05, **: p<0.01) **D)** Representative maximum intensity projections of 2-photon imaging data showing a pCX-EGFP thymic slice (green) containing CMTPX-labeled OT-II^{+} *Rag2*$^{-/-}$ *MHCII*$^{-/-}$ thymocytes (red) at 1.5h and 12h after thymocytes were added to the slices. Medullary and cortical volumes were demarcated as indicated by the masked regions. **E)** Quantification of medullary density of OT-II^{+} *Rag2*$^{-/-}$ *MHCII*$^{-/-}$ thymocytes at indicated time points after incubation on pCX-EGFP thymic slices. Individual data points represent relative medullary input cell densities from each Video compared to the average of medullary densities from all 1.5h Videos. Data were compiled from 4 time-course experiments. One-way ANOVA with Tukey's multiple comparison correction were used for statistical analysis. (Mean ± SEM; *: p<0.05, **: p<0.01, ***: p<0.001, ****: p<0.0001)

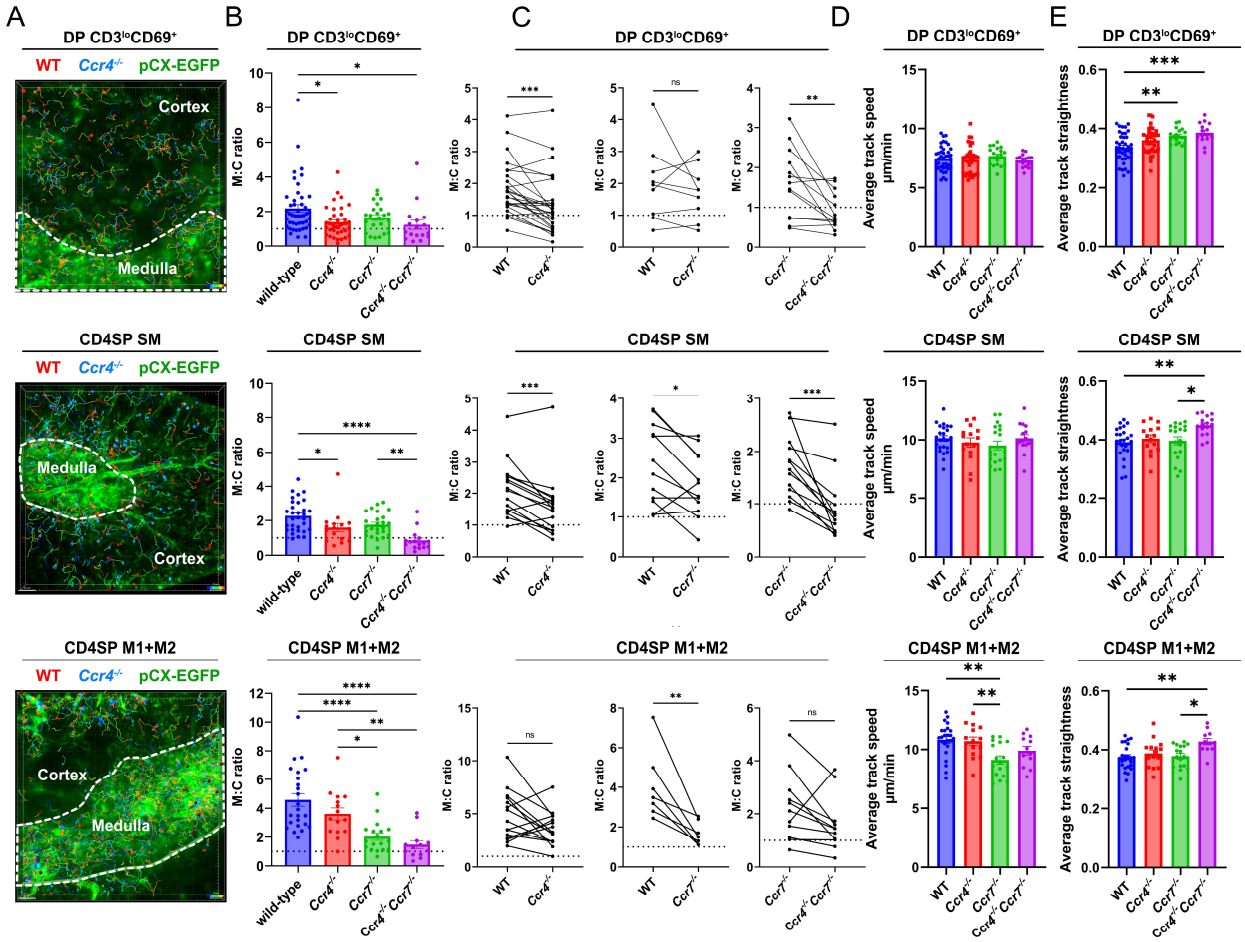

Figure 5. CCR4 and CCR7 are required for medullary accumulation of distinct post-positive selection thymocyte subsets.

A) Representative maximum intensity projections of 2-photon imaging data showing pCX-EGFP thymic slices (green) containing CMTPX (red)- and Indo-1 AM (blue)-labeled FACS sorted DP CD3^{lo}CD69^{+}, CD4SP SM or CD4SP M1+M2 cells from WT or *Ccr4*$^{-/-}$ mice, as indicated, imaged 1-4 hours after slice entry. The cortex and medulla are demarcated by white dotted lines, and cell tracks are color encoded for elapsed imaging time. **B)** Medullary-to-cortical thymocyte density ratios were quantified from 2-photon imaging data as in A), with individual data points representing ratios from individual Videos. **C)** Paired analysis of medullary-to-cortical density ratios of WT versus *Ccr4*$^{-/-}$, WT versus *Ccr7*$^{-/-}$, or *Ccr7*$^{-/-}$ versus *Ccr4*$^{-/-}$*Ccr7*$^{-/-}$ thymocyte subsets imaged simultaneously within the same slices, with individual data points representing ratios from single videos. Paired datasets are taken from the same data shown in B), and paired t-tests were used for statistical analysis. (**: p<0.01, ***: p<0.001) **D-E)** Quantification of D) average thymocyte track speeds and E) average track straightness from imaging data reported in B). Individual data points represent average track speeds or straightness of thymocytes of the indicated genotype in individual Videos. For B), D) and E), data were compiled from 19 independent experiments. One-way ANOVA with Tukey's multiple comparison correction were used for statistical analysis. (Mean ± SEM; *: p<0.05, **: p<0.01, ***: p<0.001, ****: p<0.0001)

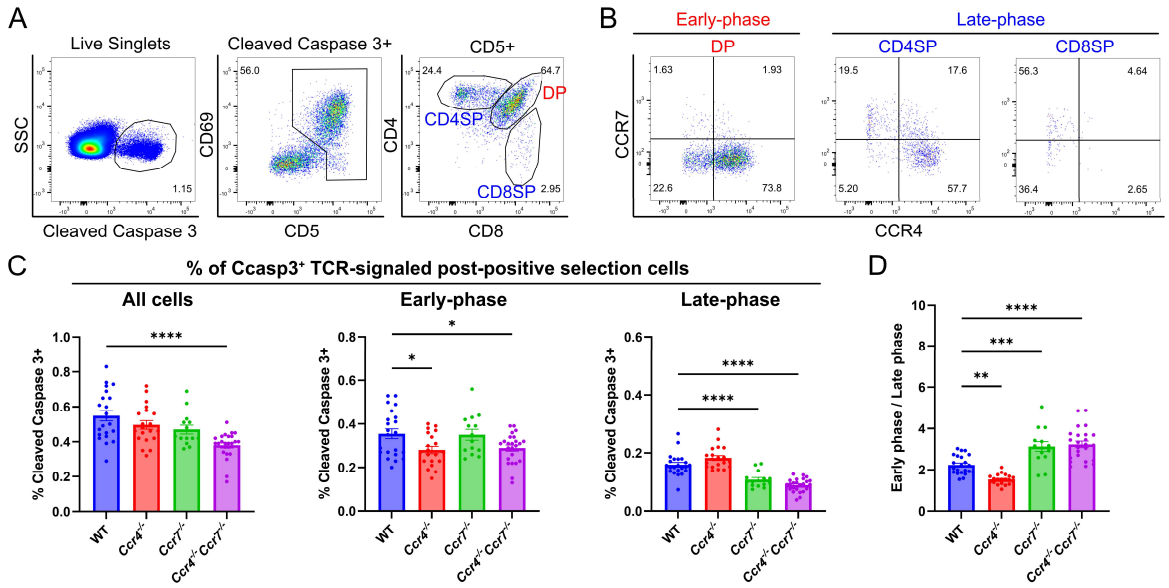

Figure 6. CCR4 and CCR7 contribute to early versus late phases of negative selection, respectively.

A) Flow cytometric gating scheme to quantify thymocytes undergoing early-phase (DP) or late-phase (CD4SP+CD8SP) negative selection. Representative data from a WT mouse is shown. **B)** Representative flow cytometry plots showing CCR4 and CCR7 expression by thymocytes undergoing early- and late-phase negative selection, as gated in C). **C)** Frequencies of total, early-phase (DP), and late-phase (CD4SP+CD8SP) negative selection among all live thymocytes in WT, *Ccr4*$^{-/-}$, *Ccr7*$^{-/-}$, and *Ccr4*$^{-/-}$*Ccr7*$^{-/-}$ mice. **D)** Ratio of thymocytes undergoing early- to late-phase negative selection in WT, *Ccr4*$^{-/-}$, *Ccr7*$^{-/-}$, and *Ccr4*$^{-/-}$*Ccr7*$^{-/-}$ mice. For C) and D), One-way ANOVA with Dunnett's multiple comparison correction were used for statistical analysis. (n=22 for WT, n=20 for *Ccr4*$^{-/-}$, n=14 for *Ccr7*$^{-/-}$, n=24 for *Ccr4*$^{-/-}$ *Ccr7*$^{-/-}$. Mean ± SEM; *: p<0.05, **: p<0.01, ***: p<0.001, ****: p<0.0001)

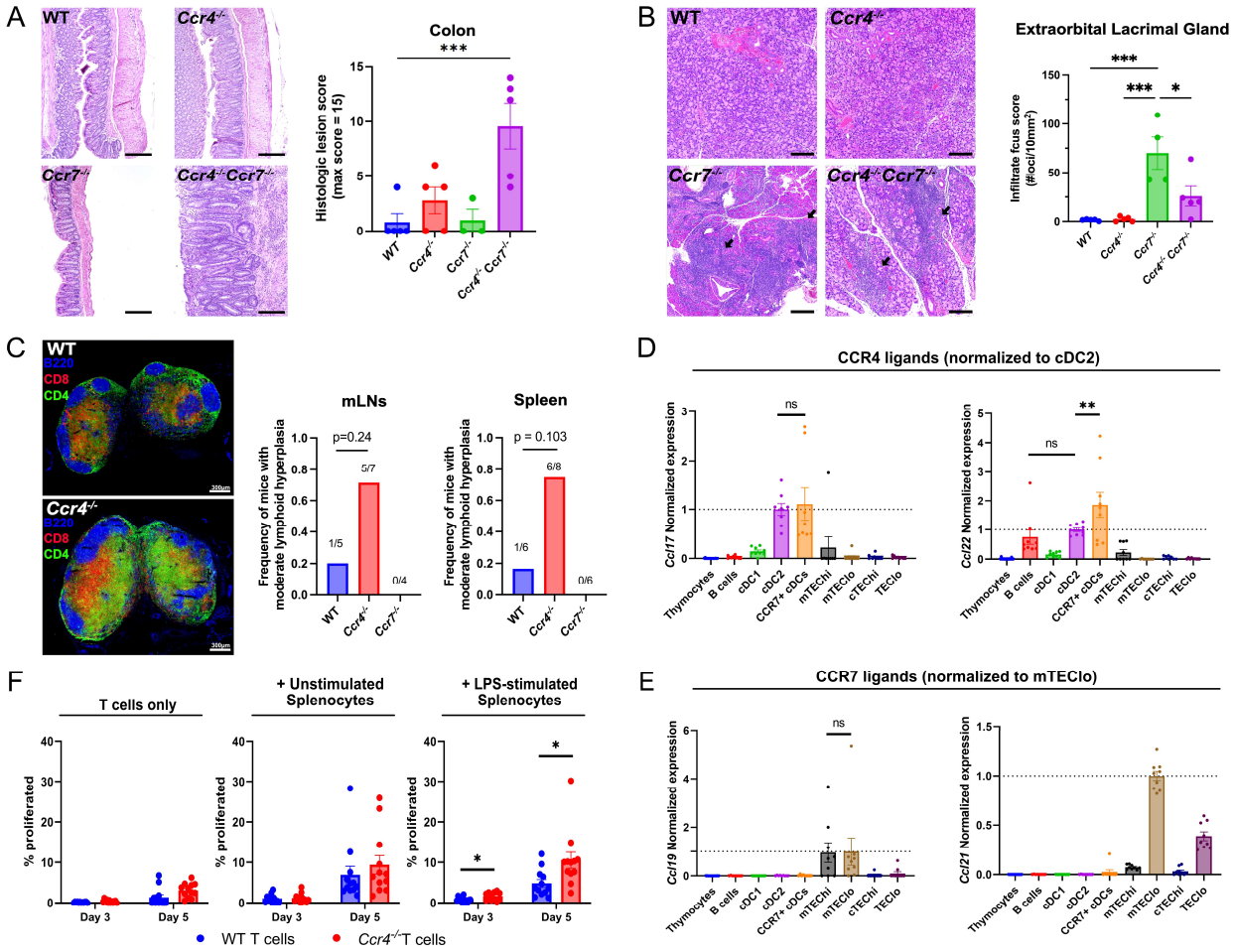

Figure 7. CCR4 and CCR7 promote tolerance to distinct organs, with CCR4 promoting tolerance to activated antigen-presenting cells.

A) Representative images of H&E stains from the colon of 5–6-month-old WT, *Ccr4*$^{-/-}$, *Ccr7*$^{-/-}$ or *Ccr4*$^{-/-}$ *Ccr7*$^{-/-}$ mice (left). Bars, 200 µm. Histological lesion score was quantified by a pathologist blinded to treatment group (right). One-way ANOVA was used to determine significance between groups (Mean ± SEM; ***: p<0.001).**B)** Representative images of H&E stains from extraorbital lacrimal glands of 5–6-month-old WT, *Ccr4*$^{-/-}$, *Ccr7*$^{-/-}$ or *Ccr4*$^{-/-}$*Ccr7*$^{-/-}$ mice (left). Bars, 500 µm. Arrows indicate lymphocytic infiltrate foci. The number of infiltrate foci per 10mm^2 was quantified (right), and one-way ANOVA was used to test significance between groups (Mean ± SEM; *: p<0.05, ***: p>0.001): C) Representative confocal images of CD4 (green), CD8 (red), and B220 (blue) on immunostained cryosections of inguinal lymph nodes from 5-6 month-old WT and *Ccr4*$^{-/-}$ mice(left). Frequency of moderate lymphoid hyperplasia in mLNs and spleens from 12-13 month-old WT, *Ccr4*$^{-/-}$and *Ccr7*$^{-/-}$ mice, as determined by a veterinary pathologist (right). Fisher's exact test was used to determine significance. **D-E)** Expression of CCR4 ligands (D) and CCR7 ligands (E) by distinct thymic antigen presenting cell subsets, assessed by qRT-PCR. Expression levels were normalized to subsets previously reported to expresses the respective ligands: CCL17 and CCL22 expression were normalized to cDC2 (Hu, Lancaster, Sasiponganan, et al., 2015), and CCL19 and CCL21 expression to mTEClo (Ki et al., 2014; Misslitz et al., 2004). Data were compiled from 3 independent experiments with triplicates. One-way ANOVA with Dunnett's multiple comparison correction were used for statistical analysis. (Mean ± SEM; ns: p>0.05, **: p<0.01) **F)** The percentage of WT or *Ccr4*$^{-/-}$ T cells that proliferated at day 3 and day 5 when cultured without

1027 splenocytes, with unstimulated splenocytes, or with LPS-stimulated splenocytes, as indicated. Data were
1028 compiled from 4 independent experiments with triplicate wells, and unpaired t-tests with Holm-Šídák's
1029 multiple comparison correction was used for statistical analysis. (Mean ± SEM; *: $p<0.05$)

1030

1031 **Supplemental Information**

1032 **Supplemental Figures and Legends**

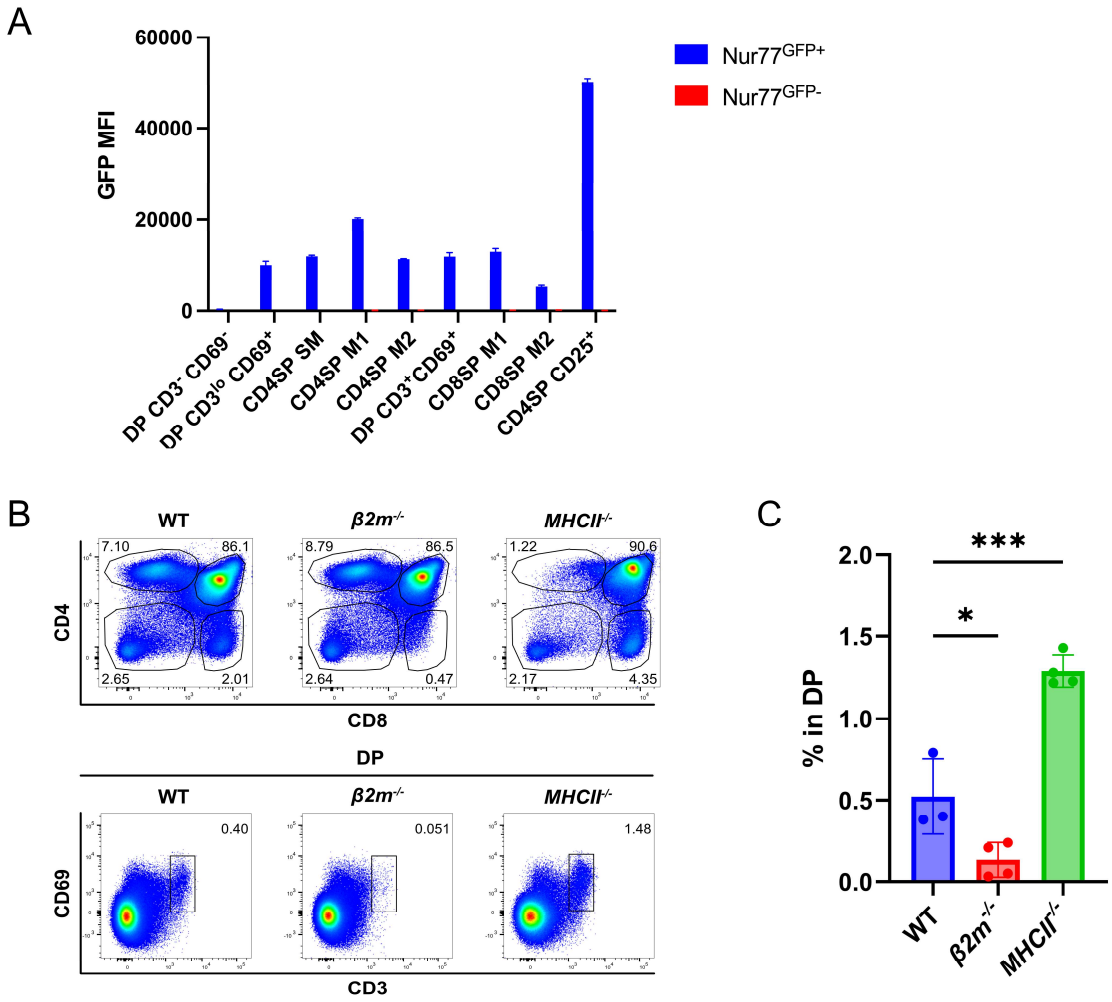

1033

1034 **Figure 1—figure supplement 1. DP CD3^{lo}CD69^{+} cells are consistent with post-positive selection DPs**
1035 **and DP CD3^{+}CD69^{+} cells represent co-receptor reversing MHCI-restricted thymocytes.**

1036 **A)** Quantification of the GFP MFI of the indicated thymocyte subsets from Nur77^{GFP} mice. Data were
1037 compiled from 3 independent experiments (Nur77^{GFP+} N=4 mice, Nur77^{GFP-} N=3 mice). **B)** Flow cytometry
1038 plots showing the absence of DP CD3^{+}CD69^{+} thymocytes from *β2m*$^{-/-}$, but not *MHCII*$^{-/-}$ thymus. **C)**
1039 Quantification of the frequency of DP CD3^{+}CD69^{+} in all DP thymocytes from wild-type, *β2m*$^{-/-}$, and *MHCII*$^{-}$
1040 $^{/-}$ mice. One-way ANOVA with Dunnett's multiple comparison correction was used for statistical analysis.
1041 (n=3 for wild-type, n=4 for *β2m*$^{-/-}$, n=3 for *MHCII*$^{-/-}$. Mean ± SEM; *: $p<0.05$, ***: $p<0.001$).

1042

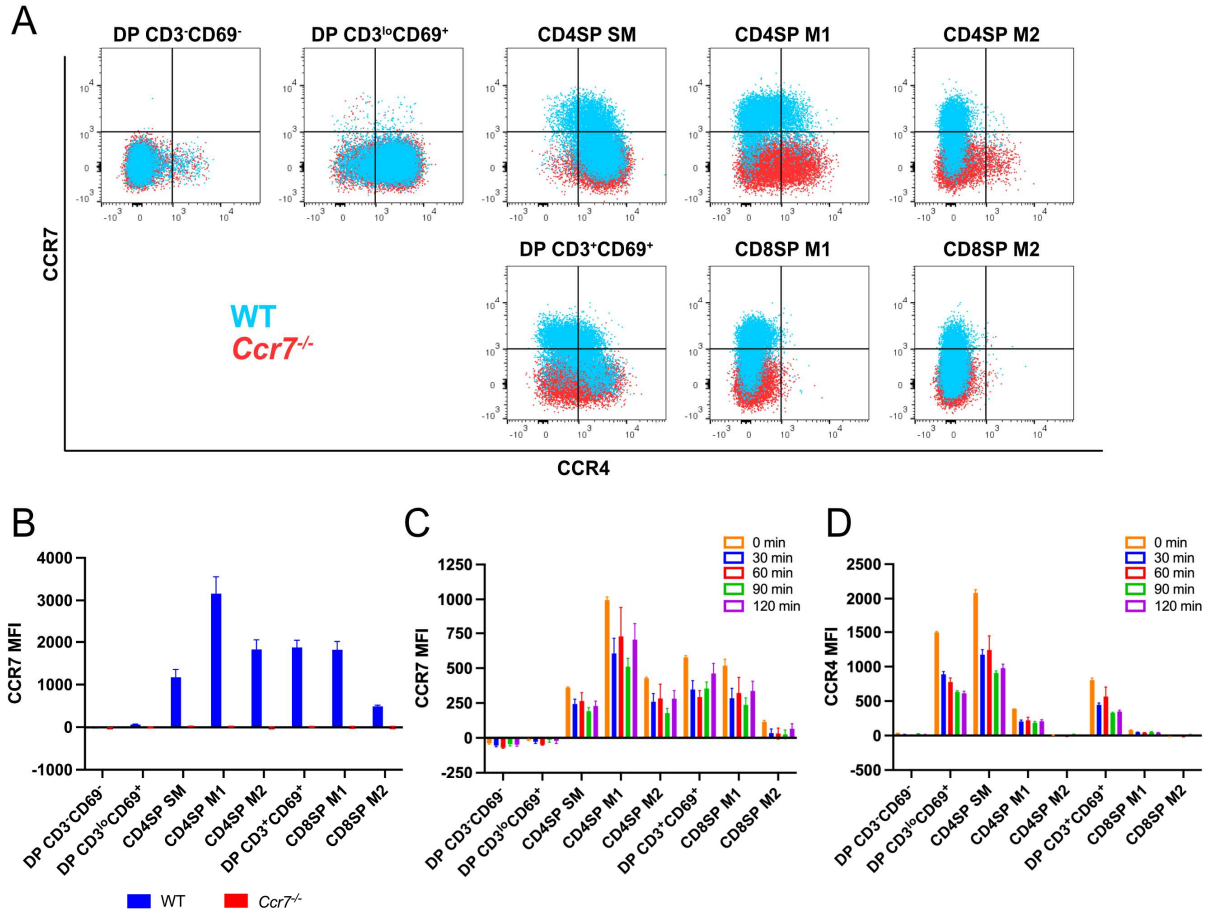

Figure 1—figure supplement 2. CCR7 expression on developing thymocytes begin at the CD4SP SM stage.

A) Representative flow cytometry overlays showing CCR4 and CCR7 expression by post-positive selection thymocyte subsets from WT and *Ccr7*$^{-/-}$ mice, respectively. **B)** Quantification of the CCR7 MFI within each subset from data in A (N = 4 mice of each genotype). **C-D)** Quantification of CCR7 and CCR4 MFIs for each thymocyte subset after incubation at 37°C for the indicated times, prior to antibody staining at 4°C. Data were compiled from 2 independent experiments (n=4 biologic replicates).

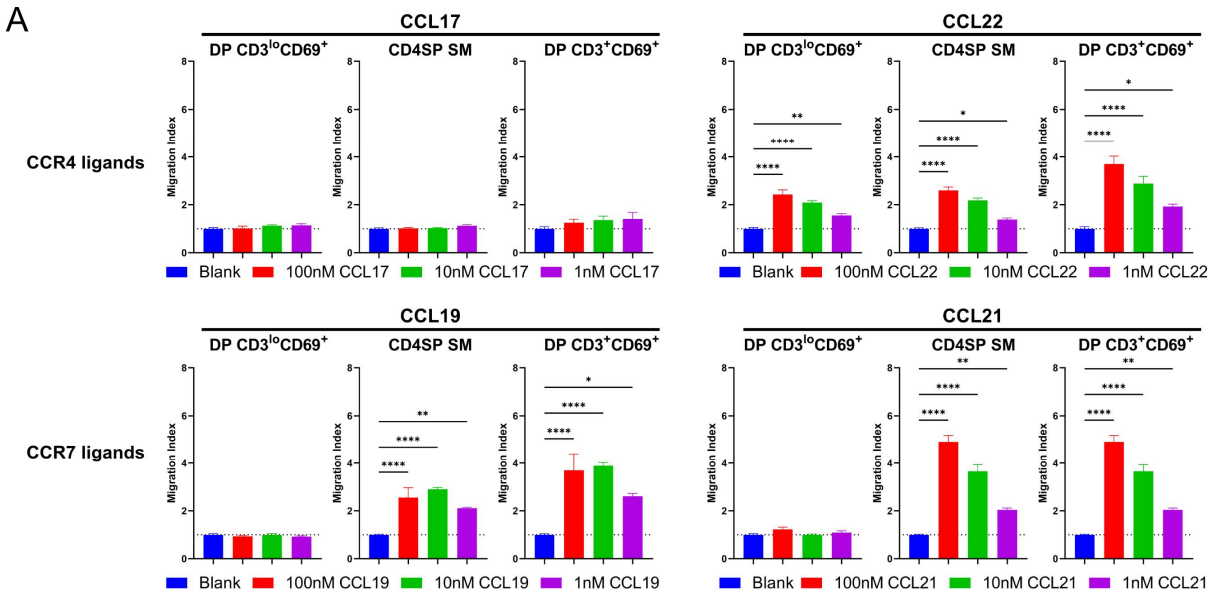

Figure 2—figure supplement 1. Chemokine signaling is not diminished in CD4SP SM thymocytes.

A) Migration indices from data in Fig. 2 for DP CD3^{lo}CD69^{+}, CD4SP SM and DP CD3^{lo}CD69^{+} were analyzed separately to compare the relative efficiency of CCR4 ligands and CCR7 ligands at inducing chemotaxis of each subset. Ordinary one-way ANOVA with Dunnett's multiple comparison corrections were used for statistical analysis. (Mean ± SEM; *: $p<0.05$, **: $p<0.01$, ***: $p<0.001$, ****: $p<0.0001$)

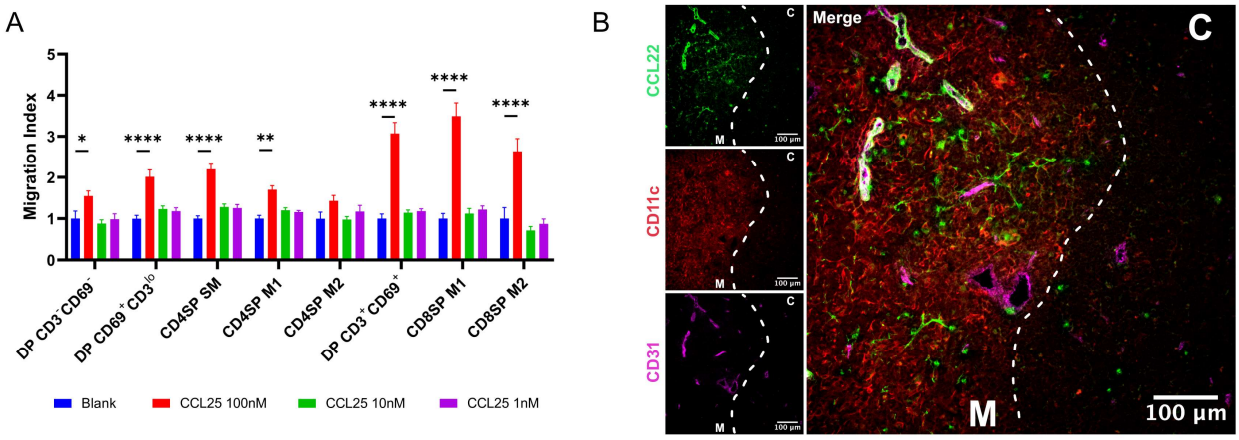

1059

1060 **Figure 2—figure supplement 2. CD4SP SM thymocytes migrate towards CCL25 and CCL22 is localized in**
1061 **the medulla.**

1062 **A)** Transwell assays were used to quantify chemotaxis of thymocyte subsets to the indicated
1063 concentrations of the CCR9 ligand, CCL25. Migration indexes were calculated as the frequencies of input
1064 cells of each subset that migrated towards the chemokine relative to the frequencies of input cells that
1065 migrated in the absence of chemokine (Blank). Data were compiled from 3 independent experiments
1066 with triplicate wells per assay. 2-way ANOVA with Dunnett's multiple comparison correction were used
1067 for statistical analysis. (Mean ± SEM; *: $p<0.05$, **: $p<0.01$, ****: $p<0.0001$). **B)** Representative confocal
1068 images of CCL22 (green), CD11c (red), and CD31 (purple) on immunostained cryosections from WT
1069 thymus. The cortex (C) and medulla (M) are demarcated by white dotted lines.

1070

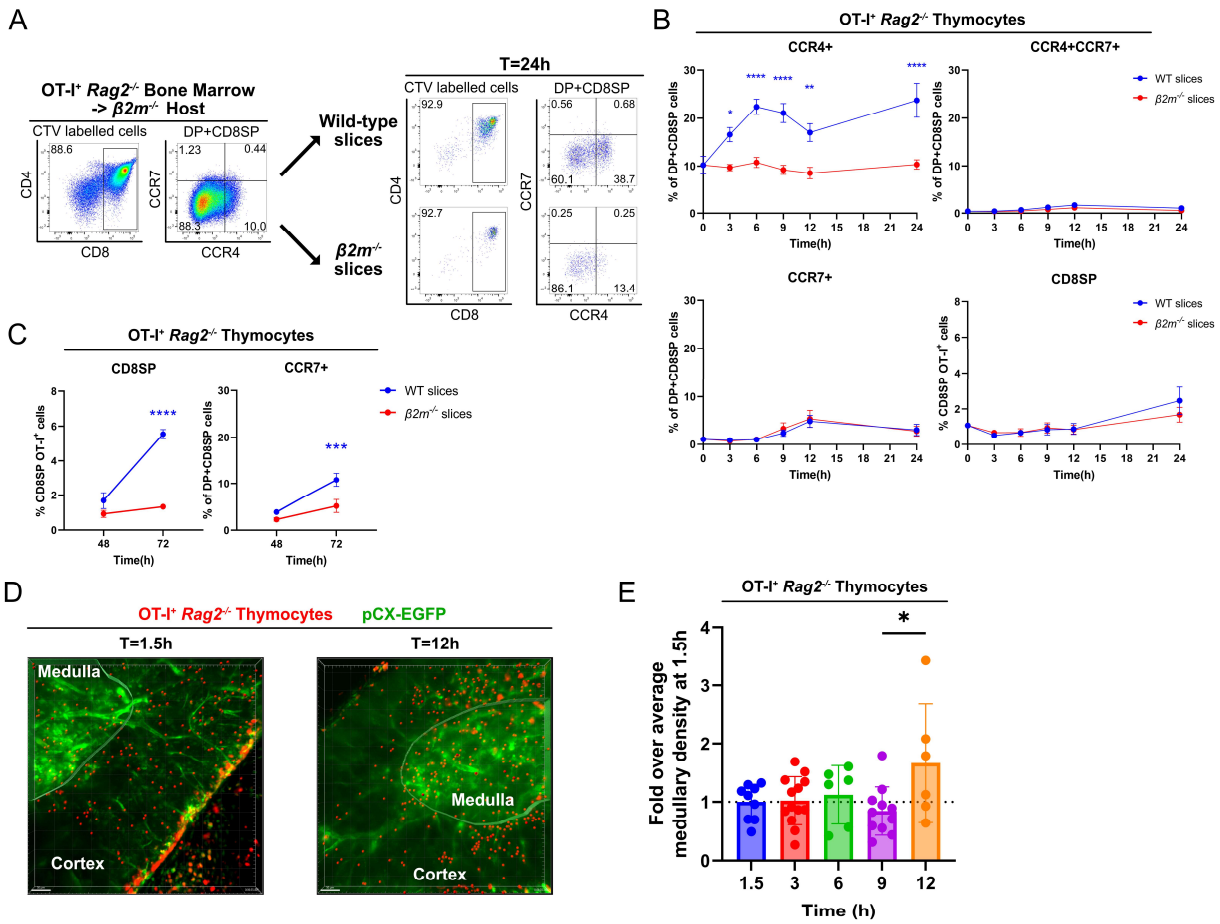

Figure 4— figure supplement 1. Rapid upregulation of CCR4 following positive selection of OT-I thymocytes correlates with medullary entry.

A) Representative flow cytometry plots of CCR4 and CCR7 expression by pre-positive selection OT-I$^+$ *Rag2*$^{-/-}$ thymocytes from *β2m*$^{-/-}$ hosts that were added to thymic slices (left) or analyzed 24h after incubation in WT or *β2m*$^{-/-}$slices, as indicated (right). **B)** Percentages of CCR4$^+$, CCR4$^+$CCR7$^+$, CCR7$^+$ or CD8SP OT-I$^+$ *Rag2*$^{-/-}$ thymocyte safter incubation on thymic slices of the indicated genotypes for the indicated time period up to 24h. **C)** Percentages of CCR7$^+$ or CD8SP OT-I$^+$ *Rag2*$^{-/-}$ thymocytes at 48h and 72h time points after initiation of thymic slices assays. Data for B-C were compiled from 3 OT-I$^+$ *Rag2*$^{-/-}$ BM -> *β2m*$^{-/-}$ experiments, with triplicate slices per experiment. Mixed-effect analysis with Šídák's multiple comparison correction were used for statistical analysis. (Mean ± SEM; *: p<0.05, **: p<0.01, ****: p<0.0001) **D)** Representative maximum intensity projections of 2-photon imaging data showing a pCX-EGFP thymic slice (green) containing CMTPX-labeled OT-I$^+$ *Rag2*$^{-/-}$ BM -> *β2m*$^{-/-}$ thymocytes (red) at 1.5h and 12h after thymocytes were added to the slices. Medullary and cortical volumes were demarcated as indicated by the masked regions. **E)** Quantification of medullary density of OT-I$^+$ *Rag2*$^{-/-}$ cells at the indicated time points. Individual data points represent medullary density calculated from each Video, relative to the average medullary density of all Videos taken at 1.5 hour. Data were compiled from 3 time-course experiments. One-way ANOVA with Tucky's multiple comparison correction were used for statistical analysis. (Mean ± SEM; *: p<0.05)

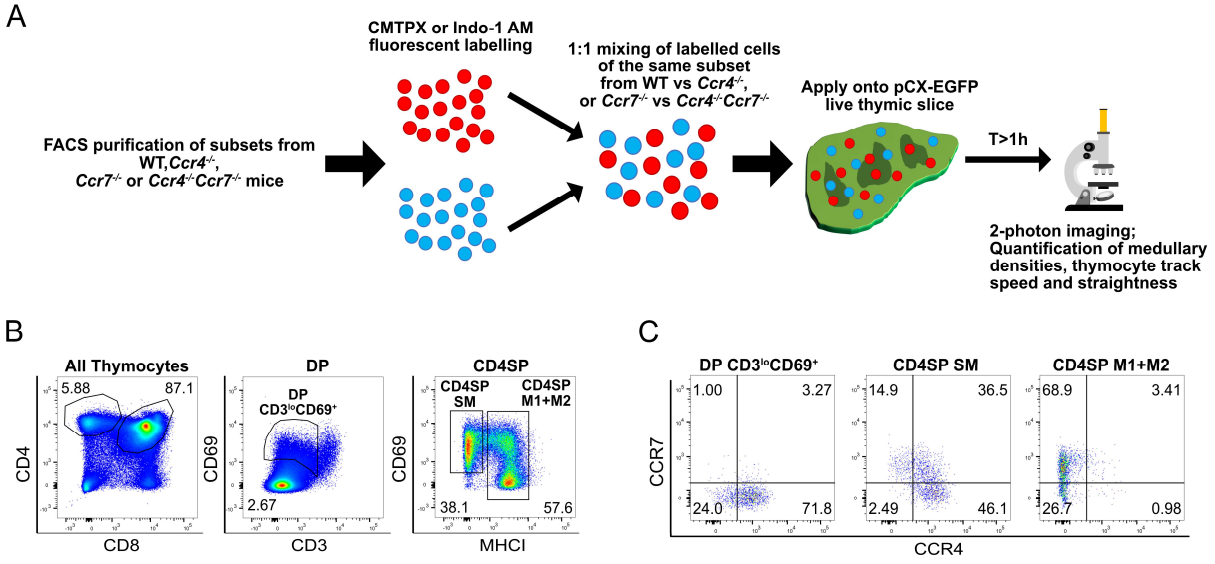

Figure 5— figure supplement 1. Experimental approach to test if CCR4 and CCR7 are required for medullary entry of distinct FACS- purified post-positive selection thymocyte subsets that differentially express CCR4 and CCR7.

A) Experimental schematic of 2-photon imaging of sorted, fluorescently labeled post-positive selection thymocyte subsets. WT cells were imaged in the same slices with *Ccr4*$^{-/-}$ or *Ccr7*$^{-/-}$ cells, and *Ccr7*$^{-/-}$ cells were imaged in the same slices with *Ccr4*$^{-/-}$ *Ccr7*$^{-/-}$ cells. Dyes were swapped between different experiments, and we did not find that use of CMTPX versus Indo-1 altered the results. **B-C)** Representative flow cytometry plots showing B) the gating scheme for sorting DP CD3^{lo}CD69^{+}, CD4SP SM and CD4SP M1+M2 subsets for 2-photon imaging, and C) CCR4 and CCR7 expression of the FACS purified thymocyte subsets from a WT mouse.

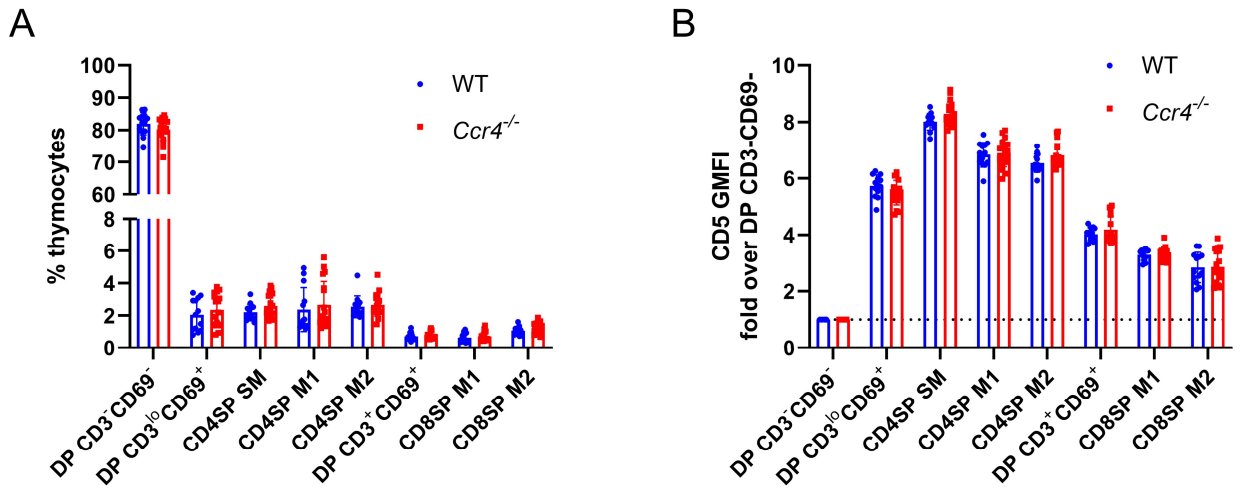

Figure 6— figure supplement 1. Thymocyte composition and CD5 levels are not altered in *Ccr4*$^{-/-}$ mice.

A) Thymocyte subset frequencies in littermate WT and *Ccr4*$^{-/-}$ mice. **B)** CD5 expression levels on the indicated thymocyte subsets from littermate WT and *Ccr4*$^{-/-}$ mice, normalized to the DP CD3^{-}CD69^{-} subset of each mouse. For A) and B), data were compiled from 6 independent experiments and significance determined using unpaired t-tests with Holm-Šídák's multiple comparison correction (Mean ± SEM; n=13 for WT, n=18 for *Ccr4*$^{-/-}$).

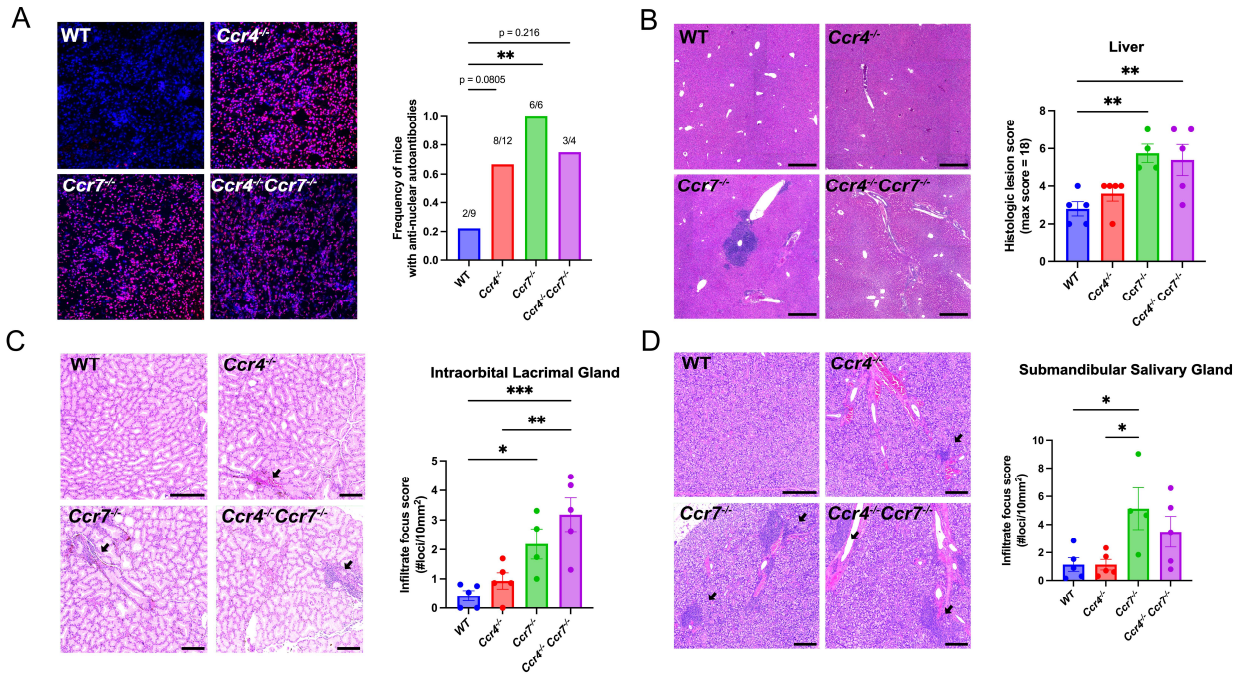

Figure 7— figure supplement 1. CCR4 and CCR7 support self-tolerance in different organs.

A) Representative images of Rag2$^{-/-}$ kidney sections immunostained with serum from 5–6.5-month-old *WT, Ccr4$^{-/-}$, Ccr7$^{-/-}$ or Ccr4$^{-/-}$Ccr7$^{-/-}$* mice (left). Anti-nuclear autoantibodies were detected as an overlay of anti–mouse IgG (red) and the nuclear DAPI stain (blue). Proportion of mice containing anti-nuclear serum autoantibodies was quantified (right). $p < 0.05$ **: $p<0.01$ (Fisher's exact test)**. B)** Representative images of H&E stains from the liver of 5–6-month-old *WT, Ccr4$^{-/-}$, Ccr7$^{-/-}$* and *Ccr4$^{-/-}$Ccr7$^{-/-}$* mice (left). Bars, 500 µm. Histological lesion score was quantified by a veterinary pathologist (right). One-way ANOVA was used to test significance between groups (Mean ± SEM; **: $p>0.01$). **C-D)** Representative images of H&E stains from intraorbital lacrimal glands (C) and submandibular salivary glands (D) of 5–6-month-old *WT, Ccr4$^{-/-}$, Ccr7$^{-/-}$ or Ccr4$^{-/-}$Ccr7$^{-/-}$* mice (left). Bars, 500 µm. Arrows indicate lymphocytic infiltrate foci. The number of infiltrate foci per 10mm^2 was quantified (right). One-way ANOVA was used to determine the significant differences between groups (Mean ± SEM; *: $p<0.05$, **: $p<0.01$, ***: $p<0.001$).

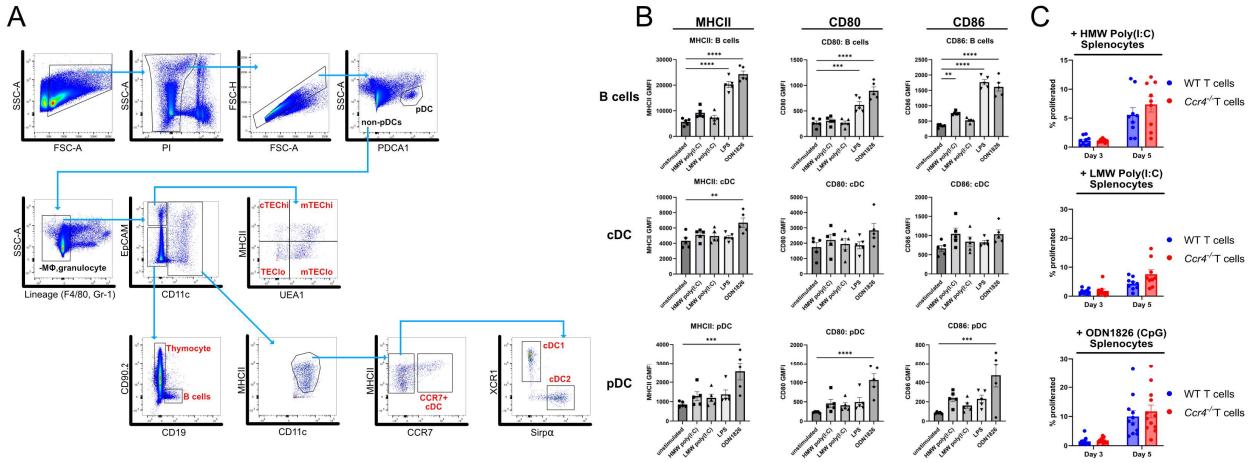

Figure 7— figure supplement 2. CCR4 promotes tolerance to activated antigen presenting cells. A) Gating scheme for FACS sorting of thymic APC subsets analyzed by qRT-PCR for expression of CCR4 and CCR7 ligands. **B)** Surface expression of MHCII, CD80 and CD86 on APC subsets from unstimulated or TLR ligand-stimulated splenocytes used in the proliferation assays in Figure 7F . Individual data points represent the GMFI of the indicated markers on each respective APC subset. Data were compiled from 5 individual experiments. One-way ANOVA with Dunnett's multiple comparison correction was used for statistical analysis. (Mean ± SEM; **: p<0.01, ***: p<0.001 ****: p<0.0001) **C)** The percentage of WT and *Ccr4*$^{-/-}$ T cells that proliferated at days 3 and 5 when cultured with High Molecular Weight (HMW) poly(I:C), Low Molecular Weight (LMW) poly(I:C), or ODN1826 (CpG)-stimulated splenocytes. Data were compiled from 3-4 independent experiments with triplicate wells, and unpaired t-tests with Holm-Šídák's multiple comparison correction was used for statistical analysis. (Mean ± SEM)

1139 **Supplemental Video Legends**

1140 **Video S1.** Two-photon live imaging of OT-II+ *Rag2*$^{-/-}$ *MHCII*$^{-/-}$ input thymocytes (red) migrating in a pCX-
1141 EGFP thymic slice (green) 1.5 hours after addition to positively selecting thymic slices, as illustrated in
1142 Figure 3D. Images were acquired for 15 minutes at 15 second time intervals through a depth of 40mm,
1143 and maximum intensity projections of input cells shown side by side.

1144

1145 **Video S2.** Two-photon live imaging of OT-II+ *Rag2*$^{-/-}$ *MHCII*$^{-/-}$ input thymocytes (red) migrating in a pCX-
1146 EGFP thymic slice (green) 12 hours after addition to positively selecting thymic slices, as illustrated in
1147 Figure 3D. Images were acquired for 15 minutes at 15 second time intervals through a depth of 40mm,
1148 and maximum intensity projections of input cells shown side by side.

1149

1150 **Video S3.** Two-photon live imaging of OT-I+ *Rag2*$^{-/-}$ input thymocytes from a *β2m*$^{-/-}$ bone marrow
1151 chimera host (red) migrating in a pCX-EGFP thymic slice (green) 1.5 hours after addition to positively
1152 selecting thymic slices, as illustrated in Supplemental Figure 3D, respectively. Images were acquired for
1153 15 minutes at 15 second time intervals through a depth of 40mm, and maximum intensity projections of
1154 input cells shown side by side.

1155

1156 **Video S4.** Two-photon live imaging of OT-I+ *Rag2*$^{-/-}$ input thymocytes from a *β2m*$^{-/-}$ bone marrow
1157 chimera host (red) migrating in a pCX-EGFP thymic slice (green) 12 hours after addition to positively
1158 selecting thymic slices, as illustrated in Supplemental Figure 3D, respectively. Images were acquired for
1159 15 minutes at 15 second time intervals through a depth of 40mm, and maximum intensity projections of
1160 input cells shown side by side.

1161

1162 **Video S5.** Two-photon live imaging of WT (red) or *Ccr4*$^{-/-}$ (blue) FACS sorted DP CD3^{lo}CD69^{+} thymocytes
1163 migrating in pCX-EGFP thymic slices (green), as illustrated in Figure 4A. Images were acquired for 15
1164 minutes at 15 second time intervals through a depth of 40mm, and maximum intensity projections of
1165 input cells with and without cell tracks, color-coded for elapsed imaging time, are shown side by side.

1166

1167 **Video S6.** Two-photon live imaging of WT (red) or *Ccr4*$^{-/-}$ (blue) FACS sorted CD4SP SM thymocytes
1168 migrating in pCX-EGFP thymic slices (green), as illustrated in Figure 4A. Images were acquired for 15
1169 minutes at 15 second time intervals through a depth of 40mm, and maximum intensity projections of
1170 input cells with and without cell tracks, color-coded for elapsed imaging time, are shown side by side.

1171

1172 **Video S7.** Two-photon live imaging of WT (red) or *Ccr4*$^{-/-}$ (blue) FACS sorted CD4SP M1+M2 thymocyte
1173 subsets, migrating in pCX-EGFP thymic slices (green), as illustrated in Figure 4A. Images were acquired
1174 for 15 minutes at 15 second time intervals through a depth of 40mm, and maximum intensity
1175 projections of input cells with and without cell tracks, color-coded for elapsed imaging time, are shown
1176 side by side.

1177

1178 **Video S8.** Two-photon live imaging of *Ccr4*$^{-/-}$*Ccr7*$^{-/-}$ (red) or *Ccr7*$^{-/-}$ (blue) FACS sorted CD4SP M1+M2
1179 subsets, migrating in pCX-EGFP thymic slices (green). Images were acquired for 15 minutes at 15 second
1180 time intervals through a depth of 40mm, and maximum intensity projections of input cells with and
1181 without cell tracks, color-coded for elapsed imaging time, are shown side by side.